In CISM Lecture Notes No. 586 "Dynamic Stability and Bifurcation in Nonconservative Mechanics" (Ch. 1), edited by:
D. Bigoni and O. Kirillov, Springer, ISBN 978-3-319-93721-2, doi 10.1007/978-3-319-93722-9

Flutter from friction in solids and structures

Davide Bigoni[*]

[*]Department of Civil, Environmental and Mechanical Engineering
University of Trento,
Via Mesiano 77 - 38123 Trento, Italy
email: davide.bigoni@unitn.it

Abstract The theory of flutter instability in structures and solids is presented, starting from the illuminating case of the Ziegler double pendulum, continuing with the Beck and Pflüger columns, and ending with the conditions for flutter in solids, considering in particular nonassociative elastoplastic models for granular and rock-like materials. The role of dissipation, leading to the so-called 'Ziegler paradox' is presented in detail. It is explained how to obtain a tangential follower load in a structure by exploiting Coulomb friction and it is shown that structures working in a flutter condition can reach a limit cycle, in which they behave as self-oscillating devices.

1 Introduction

Friction during sliding contact between solids has been usually advocated as a source of self-excited vibrations and dynamical instabilities (Den Hartog, 1956; Ibrahim, 1994a,b); examples are the violin string being excited by a bow, the brake 'squeal' (in other words, high frequency noise), the 'chatter' (low-frequency noise) produced by the cutting tool of a machine, the 'song' of a fingertip moved upon the rim of a glass of water, and the unstable fault slip in the Earth's crust, which generates an earthquake. These mechanical instabilities are often undesirable and lead to excessive damage or wear of the pieces involved in sliding, so that the principal motivation for their study is to ensure their better elimination. However, a recent approach to the mechanics of structures is their exploitation as compliant mechanisms for soft robot arms or energy harvesting devices, even in the range of large displacements and beyond critical loads. In this line of research, flutter instability could be profitably used, see for instance (Doaré and Michelin, 2011).

The most common and older explanation of these friction-related instabilities is through the introduction of stick and slip behaviour (an alternate switch between static and kinetic friction), modelled as a drop of the friction coefficient with the relative velocity of the two solids in contact. This approach was initiated by Den Hartog (1931, 1956) and generalized in different ways, see among others, Rice and Ruina (1983).

Without invoking variable friction, but rather assuming constant, time-independent, Coulomb friction, an unstable behavior has been theoretically proven (but only with reference to the linearized equations governing the problem, see Adams, 1995; Martins et al., 1999; Simões and Martins, 1998; Nguyen, 2003), so that instability appears to be intrinsically related to even the simplest model of frictional sliding. In parallel to these works, elastoplastic continua characterized by flow rule nonassociativity, the counterpart of Coulomb friction for solids, have been demonstrated to display blowing-up unstable waves, as related to the frictional behaviour of the material (Rice, 1977; Loret, 1992; Bigoni and Willis, 1994; Bigoni, 1995; Bigoni and Loret, 1999; Loret et al., 2000; Piccolroaz et al., 2006).

In all the above-mentioned works, in which instability is proven for constant friction, the concept of flutter is introduced, a nomenclature borrowed from the instability occurring in elastic structures subject to follower forces. The best known of these structures are the so-called 'Ziegler double pendulum', a 2 d.o.f. system with concentrated elasticity, and the 'Beck's column', an elastic cantilever rod subject to a tangential force at its free end. The analogy between flutter in a continuum and in a structure is more strict than it may appear at a first glance, in fact, in both cases: (i.) flutter initiates when a complex conjugate eigenvalue solution for vibrations emerges, which corresponds to an oscillation of increasing amplitude; (ii.) a necessary condition for flutter is the lack of symmetry (or self-adjointness) in the mechanical system; (iii.) in a space of parameters, flutter occurs usually within a region, which separates stability from divergence, the latter being an exponentially blowing-up motion; (iv.) flutter ultimately leads to a self-sustaining oscillation, which absorbs energy from a steady source.

In solids[1] flutter instability has been only theoretically predicted, but never experimentally detected. This was also true for the structural flutter, where the practical realization of the tangential force necessary for the insta-

[1] Kröger et al. (2008) and Neubauer et al. (2005) report examples of self-excited vibrations related to fluctuating orthogonal forces at the contact between two elements or to geometrical effects and non-conservative restoring forces. In the former case, the system is already oscillating (while the focus of this book chapter is on systems subject to a steady source of energy) and in the latter case the instability is observed in a system with finite degrees of freedom.

bility was considered the major unsolved problem[2], until Bigoni and Noselli (2011) (see also Bigoni et al., 2014, 2018) experimentally and theoretically showed how to generate a tangentially follower force in the Ziegler double pendulum through an element in sliding contact against a plate under constant Coulomb friction.

The aim of the present chapter is to review the problem of flutter instability in both structures and solids, from the specific perspective pursued by the author in the last twenty-five years. In particular, it is believed that solids and structures are akin from the point of view of flutter instability, so that they display several common features and that this instability is possible when an element draws energy from frictional sliding against another element.

The chapter is organized as follows.

- The illuminating case of the Ziegler double pendulum (Section 2.1) will show: (i.) how lack of symmetry of the geometrical stiffness matrix is responsible for flutter (Section 2.1); (ii.) why flutter cannot be detected with a quasi-static bifurcation analysis (Section 2.3); (iii.) how viscosity decreases the flutter load and (iv.) what is the so-called 'Ziegler paradox', for which a vanishing small viscosity yields a strong decrease in the flutter load (Section 2.4).
- The equations governing the dynamics of the Beck's column will be obtained from a general setting, namely, from the planar Euler elastica, in which restrictions on the magnitude of the deflection are not included (Section 2.5). The Beck's column, analyzed in a generalization given by Pflüger and including also internal and external dissipation (Section 2.7), will reveal that a continuous system displays essentially the same mechanical behaviour found for the Ziegler double pendulum, namely, that lack of symmetry (called now 'self-adjointness', Section 2.8) is a necessary condition for flutter and that the load producing the instability is significantly lowered by the presence of viscosity.

[2] Koiter (1996) proposed the 'elimination of the abstraction of follower forces as external loads from the physical and engineering literature on elastic stability' and concluded with the warning: 'beware of unrealistic follower forces'. In an attempt of realizing these forces, experiments with water or air flowing from a nozzle were conducted by Herrmann et al. (1966) and Paidoussis (2014), while a solid motor rocket was fixed at the end of an elastic column by Sugiyama et al. (1995, 2000). In the former case, there are hydrodynamical effects affecting the motion, while in the latter case the rocket has a non-negligible variable mass and burns so fast that a long-term analysis of the motion is prevented. Therefore, in both cases the follower tangential force invented by Ziegler, 1952 is not properly realized, see the exhaustive discussion by Elishakoff (2005).

- Numerical analyses will show that the dynamic motion of both the Ziegler double pendulum and the Beck's column reach a limit cycle (Section 2.9). Therefore, these structures are examples of self-oscillating mechanisms (Jenkins, 2013), in which a source of steady energy produces an oscillatory motion of given frequency. This frequency can be varied by changing the geometry and stiffness of the system.
- The possibility is shown to generate a follower force from sliding Coulomb friction (Section 2.10), a concept introduced by Bigoni and Noselli (2011), which is based on an extreme form of orthotropic friction, null in the direction orthogonal to the sliding. It is also anticipated that a device similar to that employed for the Ziegler double pendulum can be designed to produce flutter instability in the Beck and Pflüger rods (Bigoni et al., 2018).
- The behaviour of a continuous elastoplastic material, in which the yielding is pressure-sensitive and the plastic flow nonassociative, is introduced (Section 3) from a simple 2 d.o.f. model of contact with Coulomb friction (Section 3.1).
- With reference to nonassociative and pressure-sensitive elastoplastic solids, the problem of plane waves is solved with reference to the loading branch of the constitutive operator[3] and is shown to be governed by the eigenvalues of the acoustic tensor (Section 3.3). Strain localization into planar bands is explained in terms of vanishing of an eigenvalue of the acoustic tensor (Section 3.4). The conditions for flutter instability in the above-mentioned solids are finally analyzed (Section 3.5) and it is explained that this instability has to be considered more frequent than it is usually believed.
- As conclusions, a discussion on the state-of-the-art and the perspectives in the research on flutter instability in solids and structures is reported (Section 4).

2 Flutter for structural systems

Flutter in structural systems is analyzed under the hypothesis that follower forces are present. In general, these forces do not admit a potential and therefore are non-conservative, so that work can be extracted in a closed

[3] The treatment is limited to the linearized version of contact with friction and to the linearized incremental plasticity, so that the complex role of nonlinarity is not considered for simplicity. The interested reader is addressed to Bigoni and Petryk (2002) for further details on this delicate issue.

path of deformation. This can easily be understood with reference to the two structures shown in Fig. 1. One of these structures is made up of two rigid bars jointed together with a hinge and constrained with another hinge at one end, while at the other end a load is applied, which remains coaxial with the bar to which it is applied. The other structure is a clamped elastic rod subject to a force, which remains tangential to the elastica at the free end. The load, as illustrated in the figure caption, is capable of producing a positive work in a closed deformation loop.

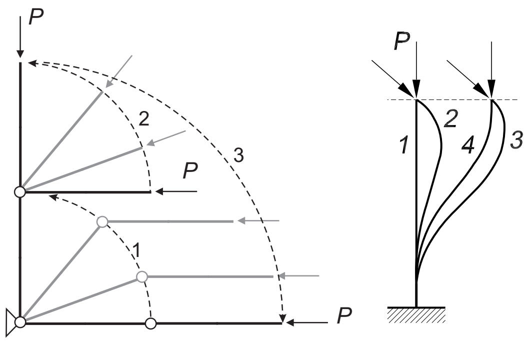

Figure 1. A tangential follower force is applied: (left) at the right end of a two-degree-of-freedom system composed by two hinged rigid bars; (right) at the free end of a clamped elastic rod. The load is not conservative, since in the closed loops $1 \longrightarrow 2 \longrightarrow 3$ (for the structure on the left) and $1 \longrightarrow 2 \longrightarrow 3, \longrightarrow 4, \longrightarrow 1$, (for the structure on the right) a positive work is produced by the applied force. The deformation loop sketched in the deformable rod shown on the right is based on a small displacement assumption and consists in a rotation of the loaded end ($1 \longrightarrow 2$, during which the load does not work), which is followed by a translation of the end ($2 \longrightarrow 3$, during which a positive work is produced), by another rotation at fixed position ($3 \longrightarrow 4$, during which the load does not work), and, finally, by an horizontal translation back to the initial position ($4 \longrightarrow 1$, during which work is not produced).

2.1 The Ziegler double pendulum

Flutter and divergence instability can be vividly and simply illustrated with reference to a structure, invented more than sixty years ago by Ziegler (1952, 1977). The structure is the double pendulum shown in Fig. 2, made up of two rigid bars, connected through an elastic hinge and fixed with another elastic hinge at one end. The structure is subject to a tangential follower load on the free end, which remains coaxial to the second rigid rod and can produce positive work in a closed loop (as explained in Fig. 1).

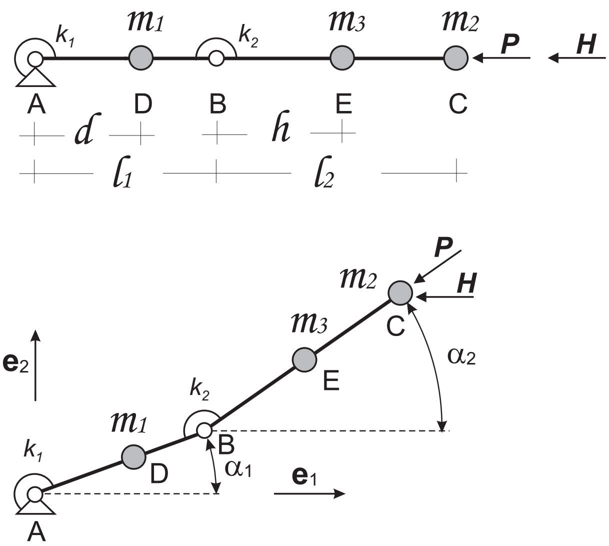

Figure 2. The Ziegler double pendulum, namely, a two-degree-of-freedom system subject to a follower (non-conservative) load (the force **P**, applied at C, remains always parallel to the rod BC). In addition, a dead (conservative) load (the force **H**, applied at C, remains always parallel to $\mathbf{e}_1$) is also included for reference. The rods are rigid and massless and connected with two springs of stiffness k_1 and k_2; three concentrated masses m_1, m_2, and m_3 are present. Two cases will be analyzed, $\mathbf{H} = 0$ corresponding to purely follower load and $\mathbf{P} = 0$ corresponding to purely conservative load. In the former case, quasi-static bifurcation is excluded, but flutter and divergence instability will be shown to be always possible for sufficiently high **P**. In the latter case, quasi-static bifurcation occurs and only divergence instability is possible.

Subject to the follower load, the Ziegler double pendulum (Fig. 2) is considered, where two rotational springs of stiffnesses k_1 and k_2 provide the elasticity and three concentrated masses the inertia. The generic configuration of the system remains determined by the two Lagrangean parameters α_1 and α_2. The concentrated masses m_1 and m_3 are located at the points D and E, at a distance d from A and h from B, while the concentrated mass

m_2 is located at C. The tangential follower load $\mathbf{P}$, applied at C and taken positive when compressive, maintains the direction parallel to the rod BC. In addition to this force, a second load, produced by a conservative dead force $\mathbf{H}$, is also applied at C. The analysis of a mechanical system similar to that under consideration (in which the mass m_3 is not present) can be found in (Herrmann, 1971; Ziegler, 1952, 1953, 1956, 1977; Nguyen, 1995).

Governing equations for the double pendulum A simple static analysis of the structure shown in Fig. 2 is sufficient to conclude that only the trivial (straight) configuration satisfies equilibrium when only the follower load $\mathbf{P}$ is applied (in fact equilibrium of the rod BC is only possible if $\alpha_1 = \alpha_2$, and equilibrium of the complex ABC additionally requires $\alpha_1 = 0$), so that quasi-static bifurcations are excluded. Therefore, flutter and divergence instabilities, which will be found to occur in the Ziegler double pendulum, necessary represent dynamical instabilities, the former will be shown to consist in an oscillatory vibration of increasing amplitude, while the latter in an exponentially growing motion. Note that the situation changes when only the dead load $\mathbf{H}$ is applied, in which case non-trivial equilibrium configurations and therefore quasi-static bifurcations are possible.

The equations of motion for the system can be obtained starting from the position vectors of the three concentrated masses m_1, m_2 and m_3

$$
\begin{aligned}
\mathbf{D}-\mathbf{A} &= d\cos\alpha_1\mathbf{e}_1 + d\sin\alpha_2\mathbf{e}_2,\\
\mathbf{E}-\mathbf{A} &= (l_1\cos\alpha_1 + h\cos\alpha_2)\,\mathbf{e}_1 + (l_1\sin\alpha_1 + h\sin\alpha_2)\,\mathbf{e}_2,\\
\mathbf{C}-\mathbf{A} &= (l_1\cos\alpha_1 + l_2\cos\alpha_2)\,\mathbf{e}_1 + (l_1\sin\alpha_1 + l_2\sin\alpha_2)\,\mathbf{e}_2,
\end{aligned}
\tag{1}
$$

where $\mathbf{e}_1$ and $\mathbf{e}_2$ are the two unit vectors singling out the horizontal and vertical directions respectively, so that the forces $\mathbf{P}$ and $\mathbf{H}$, of moduli P and H, can be expressed as

$$
\mathbf{P} = -P\cos\alpha_2\mathbf{e}_1 - P\sin\alpha_2\mathbf{e}_2, \qquad \mathbf{H} = -H\mathbf{e}_1. \tag{2}
$$

The velocities of points $\mathbf{D}$, $\mathbf{C}$, and $\mathbf{E}$ (the time derivative is denoted by a superimposed dot) are

$$
\begin{aligned}
\dot{\mathbf{D}} &= -d\left(\dot{\alpha}_1 \sin\alpha_1 \mathbf{e}_1 - \dot{\alpha}_1 \cos\alpha_1 \mathbf{e}_2\right), \\
\dot{\mathbf{C}} &= \left(-l_1\dot{\alpha}_1 \sin\alpha_1 - l_2\,\dot{\alpha}_2 \sin\alpha_2\right)\mathbf{e}_1 \\
&\qquad\qquad + \left(l_1\dot{\alpha}_1 \cos\alpha_1 + l_2\,\dot{\alpha}_2 \cos\alpha_2\right)\mathbf{e}_2, \\
\dot{\mathbf{E}} &= \left(-l_1\dot{\alpha}_1 \sin\alpha_1 - h\,\dot{\alpha}_2 \sin\alpha_2\right)\mathbf{e}_1 \\
&\qquad\qquad + \left(l_1\dot{\alpha}_1 \cos\alpha_1 + h\,\dot{\alpha}_2 \cos\alpha_2\right)\mathbf{e}_2,
\end{aligned}
\tag{3}
$$

so that the accelerations $\ddot{\mathbf{D}}$, $\ddot{\mathbf{C}}$ and $\ddot{\mathbf{E}}$ of the masses m_1, m_2 and m_3 can be evaluated as

$$
\begin{aligned}
\ddot{\mathbf{D}} &= -d\left(\dot{\alpha}_1^2 \cos\alpha_1 + \ddot{\alpha}_1 \sin\alpha_1\right)\mathbf{e}_1 - d\left(\dot{\alpha}_1^2 \sin\alpha_1 - \ddot{\alpha}_1 \cos\alpha_1\right)\mathbf{e}_2, \\
\ddot{\mathbf{C}} &= \left(-l_1\dot{\alpha}_1^2 \cos\alpha_1 - l_1\ddot{\alpha}_1 \sin\alpha_1 - l_2\,\dot{\alpha}_2^2 \cos\alpha_2 - l_2\,\ddot{\alpha}_2 \sin\alpha_2\right)\mathbf{e}_1 \\
&\quad + \left(-l_1\dot{\alpha}_1^2 \sin\alpha_1 + l_1\ddot{\alpha}_1 \cos\alpha_1 - l_2\,\dot{\alpha}_2^2 \sin\alpha_2 + l_2\,\ddot{\alpha}_2 \cos\alpha_2\right)\mathbf{e}_2, \\
\ddot{\mathbf{E}} &= \left(-l_1\dot{\alpha}_1^2 \cos\alpha_1 - l_1\ddot{\alpha}_1 \sin\alpha_1 - h\,\dot{\alpha}_2^2 \cos\alpha_2 - h\,\ddot{\alpha}_2 \sin\alpha_2\right)\mathbf{e}_1 \\
&\quad + \left(-l_1\dot{\alpha}_1^2 \sin\alpha_1 + l_1\ddot{\alpha}_1 \cos\alpha_1 - h\,\dot{\alpha}_2^2 \sin\alpha_2 + h\,\ddot{\alpha}_2 \cos\alpha_2\right)\mathbf{e}_2.
\end{aligned}
\tag{4}
$$

Noting that the moments transmitted by the rotational springs to the rods are $k_1\alpha_1$ and $k_2(\alpha_2 - \alpha_1)$, the principle of virtual power writes as

$$
\begin{aligned}
&(\mathbf{P} + \mathbf{H}) \cdot \delta\mathbf{C} - m_1\ddot{\mathbf{D}} \cdot \delta\mathbf{D} - m_2\ddot{\mathbf{C}} \cdot \delta\mathbf{C} - m_3\ddot{\mathbf{E}} \cdot \delta\mathbf{E} \\
&\qquad\qquad - k_1\alpha_1\delta\alpha_1 - k_2(\alpha_2 - \alpha_1)(\delta\alpha_2 - \delta\alpha_1) = 0,
\end{aligned}
\tag{5}
$$

where '$\cdot$' denotes the scalar product and the virtual velocities $\delta\mathbf{C}$, $\delta\mathbf{D}$, $\delta\mathbf{E}$ have the same expressions provided by equations (3) with the '$\dot{}$' replaced by 'δ'.

The virtual power of the external loads is

$$
(\mathbf{P} + \mathbf{H}) \cdot \delta\mathbf{C} = Pl_1 \sin(\alpha_1 - \alpha_2)\delta\alpha_1 + H\left(l_1\delta\alpha_1 \sin\alpha_1 + l_2\,\delta\alpha_2 \sin\alpha_2\right). \tag{6}
$$

It is noted that, while the conservative load H admits the potential

$$
W(\alpha_1, \alpha_2) = H\left(l_1 \cos\alpha_1 + l_2 \cos\alpha_2 - l_1 - l_2\right), \tag{7}
$$

so that

$$\mathbf{H} \cdot \delta \mathbf{C} = -\frac{\partial W}{\partial \alpha_1}\delta\alpha_1 - \frac{\partial W}{\partial \alpha_2}\delta\alpha_2, \tag{8}$$

the nonconservative force P does not admit one, as demonstrated by the condition

$$\frac{\partial \sin(\alpha_1 - \alpha_2)}{\partial \alpha_2} \neq \frac{\partial 0}{\partial \alpha_1}. \tag{9}$$

Imposing now the virtual power equation (5) and invoking the arbitrariness of $\delta\alpha_1$ and $\delta\alpha_2$ yields the two equations

$$\boxed{\begin{aligned}
&\left[m_1 d^2 + (m_2+m_3)l_1^2\right]\ddot{\alpha}_1 + (m_2 l_2 + m_3 h) l_1 \ddot{\alpha}_2 \cos(\alpha_1-\alpha_2) \\
&+(m_2 l_2 + m_3 h) l_1 \dot{\alpha}_2^2 \sin(\alpha_1-\alpha_2) + k_1\alpha_1 + k_2(\alpha_1-\alpha_2) \\
&\qquad\qquad -P l_1 \sin(\alpha_1-\alpha_2) - H l_1 \sin\alpha_1 = 0, \\
&(m_2 l_2 + m_3 h) l_1 \ddot{\alpha}_1 \cos(\alpha_1-\alpha_2) + (m_2 l_2^2 + m_3 h^2)\ddot{\alpha}_2 \\
&-(m_2 l_2 + m_3 h) l_1 \dot{\alpha}_1^2 \sin(\alpha_1-\alpha_2) - k_2(\alpha_1-\alpha_2) \\
&\qquad\qquad\qquad\qquad -H l_2 \sin\alpha_2 = 0,
\end{aligned}} \tag{10}$$

governing the (nonlinear) dynamics of the system.

The differential equations (10), linearized near the trivial (equilibrium) configuration $\alpha_1 = \alpha_2 = 0$, can be written, in matrix form, as

$$\begin{aligned}
&\underbrace{\begin{bmatrix} m_1 d^2 + (m_2+m_3)l_1^2 & (m_2 l_2 + m_3 h) l_1 \\ (m_2 l_2 + m_3 h) l_1 & m_2 l_2^2 + m_3 h^2 \end{bmatrix}}_{mass\ matrix} \begin{bmatrix} \ddot{\alpha}_1 \\ \ddot{\alpha}_2 \end{bmatrix} \\
&+ \left(\overbrace{\begin{bmatrix} k_1 + k_2 & -k_2 \\ -k_2 & k_2 \end{bmatrix}}^{stiffness\ matrix} + \overbrace{\begin{bmatrix} -l_1(P-H) & P l_1 \\ 0 & -H l_2 \end{bmatrix}}^{geometric\ matrix} \right) \begin{bmatrix} \alpha_1 \\ \alpha_2 \end{bmatrix} = 0.
\end{aligned} \tag{11}$$

Note that the mass matrix and the stiffness matrix are both real, symmetric, and positive definite, while the geometric matrix is real, but unsymmetric, thus introducing the only source of unsymmetry. More specifically, the unsymmetry comes *only* from the presence of the follower load P, but not from the dead load H.

Time-harmonic vibrations of the double pendulum Looking for time-harmonic vibrations near the equilibrium configuration, the Lagrangean parameters α_j are assumed to be harmonic functions of time

$$\alpha_j = a_j\, e^{-i\Omega\, t}, \quad j = 1, 2, \tag{12}$$

where a_j are (complex) amplitudes, Ω is the (possibly complex) circular frequency, and i is the imaginary unit ($i = \sqrt{-1}$), so that a substitution of equations (12) into equations (11) yields

$$\begin{aligned} &\left(\begin{bmatrix} k_1 + k_2 - l_1(P + H) & -k_2 + Pl_1 \\ \\ -k_2 & k_2 - Hl_2 \end{bmatrix} \right. \\ &\left. -\Omega^2 \begin{bmatrix} m_1 d^2 + (m_2 + m_3) l_1^2 & (m_2 l_2 + m_3 h) l_1 \\ \\ (m_2 l_2 + m_3 h) l_1 & m_2 l_2^2 + m_3 h^2 \end{bmatrix} \right) \begin{bmatrix} a_1 \\ \\ a_2 \end{bmatrix} = 0. \end{aligned} \tag{13}$$

The algebraic system (13) represents a generalized eigenvalue problem for Ω^2, that after introducing the mass $\mathbf{M}$, the stiffness $\mathbf{K}$, and geometric $\mathbf{G}$ matrices, can be written as

$$\left[\mathbf{K} + \mathbf{G} - \Omega^2 \mathbf{M}\right] \mathbf{a} = 0, \tag{14}$$

which would be a standard eigenvalue problem if $\mathbf{M}$ would be equal to the identity. However, the mass matrix $\mathbf{M}$ is real, symmetric and positive definite, so that its square root $\mathbf{M}^{1/2}$ (defined in such a way that $\mathbf{M}^{1/2}\mathbf{M}^{1/2} = \mathbf{M}$) is invertible. Therefore, the generalized eigenvalue problem (14) can be rewritten as

$$\left[(\mathbf{K} + \mathbf{G})\, \mathbf{M}^{-1/2} - \Omega^2 \mathbf{M}^{1/2}\right] \mathbf{M}^{1/2}\mathbf{a} = 0. \tag{15}$$

Therefore a multiplication by $\mathbf{M}^{-1/2}$ transforms the nonstandard eigenvalue (14) into a standard one

$$\left[\mathbf{M}^{-1/2}\, (\mathbf{K} + \mathbf{G})\, \mathbf{M}^{-1/2} - \Omega^2 \mathbf{I}\right] \mathbf{M}^{1/2}\mathbf{a} = 0, \tag{16}$$

where the matrix $\mathbf{M}^{-1/2}\, (\mathbf{K} + \mathbf{G})\, \mathbf{M}^{-1/2}$ is not symmetric because of the unsymmetry of $\mathbf{G}$, which in turn follows from the presence of the follower load P. It can be concluded from equation (16) that:

a necessary condition for the eigenvalues Ω^2 to be complex conjugate (a situation which will be identified with the flutter instability) is that the geometric matrix $\mathbf{G}$ *be unsymmetric, otherwise, if* $\mathbf{G}$ *is symmetric, the eigenvalues will always be real.*

A generalization to n d.o.f. The generalized eigenvalue problem (14) applies to all mechanical systems (with smooth and bilateral constraints) with finite, say n, degrees of freedom. The mass matrix $\mathbf{M}$ becomes $n \times n$, but remains symmetric and positive definite, so that the generalized eigenvalue problem can be cast in the standard form (16), where now all matrices are $n \times n$. The stiffness matrix is also symmetric and positive definite, therefore the only possible source of unsymmetry remains $\mathbf{G}$, so that it may be concluded that in all cases where $\mathbf{G}$ is symmetric, complex conjugate eigenvalues (and therefore flutter instability) are excluded.

2.2 The standard case as a reference: the dead load H on the double pendulum

Assuming that the double pendulum is loaded only with the dead loading $\mathbf{H}$, so that $\mathbf{P} = 0$, and introducing now the dimensionless variables,

$$\begin{aligned} &\rho_1 = \frac{m_1}{m_2}, \quad \rho_2 = \frac{m_3}{m_2}, \quad y_1 = \frac{d}{l_1}, \quad y_2 = \frac{h}{l_2}, \\ &\lambda = \frac{l_1}{l_2}, \quad k = \frac{k_1}{k_2}, \quad \omega^2 = \frac{m_2 l_2^2 \Omega^2}{k_2}, \quad \eta = \frac{H l_1}{k_2}, \end{aligned} \tag{17}$$

matrix $\mathbf{G}$ becomes symmetric (so that complex eigenvalues are excluded) and the generalized eigenvalue problem (13) can be compacted so that the matrix multiplying vector $[a_1, a_2]$ is now

$$\begin{bmatrix} (\rho_1 y_1^2 + \rho_2 + 1)\lambda^2\omega^2 - 1 - k + \eta & \lambda\,\omega^2(1 + \rho_2 y_2) + 1 \\ \lambda\,\omega^2(1 + \rho_2 y_2) + 1 & \omega^2(1 + \rho_2 y_2^2) - 1 + \eta/\lambda \end{bmatrix}, \tag{18}$$

and nontrivial solutions become possible when its determinant vanishes, a condition providing

$$\omega^2 = \frac{\beta_1 - \eta\delta_2 \pm \sqrt{\Delta(\eta)}}{2a}, \tag{19}$$

where the discriminant is

$$\Delta(\eta) = (\beta_1 - \eta\delta_2)^2 - 4ac(\eta), \tag{20}$$

and

$$\begin{aligned}
&a = \lambda^2 \left[y_1^2\rho_1 + (1-y_2)^2\rho_2 + y_1^2 y_2^2 \rho_1\rho_2\right] > 0, \\
&\beta_1 = \lambda\left[2 + 2y_2\rho_2 + \lambda(1 + y_1^2\rho_1 + \rho_2)\right] + (k+1)(1+\rho_2 y_2^2) > 0, \\
&\delta_2 = 1 + \lambda(1 + y_1^2\rho_1 + \rho_2) + \rho_2 y_2^2 > 0, \\
&c(\eta) = \eta^2/\lambda - \eta(1 + 1/\lambda + k/\lambda) + k,
\end{aligned} \tag{21}$$

Now the problem (13) is symmetric, because follower forces are absent, so that $\Delta(\eta)$ cannot be negative. Therefore, two solutions for ω^2 remain positive for loads inferior to the critical load, namely, to the smaller, H_{cr}, of the two buckling loads

$$\left.\begin{array}{c}\dfrac{H_{cr} l_1}{k_2} \\[2ex] \dfrac{H_{sup} l_1}{k_2}\end{array}\right\} = \frac{1 + k + \lambda \mp \sqrt{(\lambda - k)^2 + 1 + 2k + 2\lambda}}{2} > 0. \tag{22}$$

At H_{cr}, and also at H_{sup}, one of the solutions for ω^2 vanishes, so that the critical load coincides with that calculated using the static method, because at H_{cr} and at H_{sup} the matrix (18) becomes singular for $\omega = 0$ and its determinant is $c(\eta)$.

For loads H higher than the critical load, the solutions ω^2 become:

$$\begin{aligned}
&\text{– one positive and one negative when:} \quad && H \in (H_{cr}, H_{sup}), \\
&\text{– two negative when:} && H > H_{sup}.
\end{aligned} \tag{23}$$

As a consequence, the four solutions Ω

$$\Omega = \pm\frac{1}{l_2}\sqrt{\frac{k_2}{m_2}}\sqrt{\frac{\beta_1 - \eta\delta_2 \pm \sqrt{(\beta_1 - \eta\delta_2)^2 - 4ac(\eta)}}{2a}}, \tag{24}$$

are all four real for loads smaller than H_{cr}, two real and two forming one purely imaginary complex conjugate pair for loads higher than H_{cr}, but smaller than H_{sup}, and four split into two purely imaginary complex conjugate pairs at a load higher than H_{sup}.

The purely imaginary complex pair always contains an element which, multiplied by $-i$, provides an exponentially blowing-up solution, which corresponds to *divergence instability*. Therefore, for dead load, either stability or divergence instability may only occur.

Note that, as a particular case, the critical load (22) for $k_1 = k_2 = K$ and $l_1 = l_2 = L$ ($\lambda = 1$) simplifies to

$$H_{cr} = \frac{(3 - \sqrt{5})K}{2L} \approx 0.382 \frac{K}{L}. \tag{25}$$

The effect of viscosity on the buckling of the double pendulum subject only to dead loading H can be investigated assuming that the two elastic hinges become viscoelastic. Viscosity reacts to an angular relative velocity of the connected rods with a couple, so that, denoting with c_1 and c_2 the two coefficients of viscosity of the hinges, equation (11) is modified through the addiction of the term

$$\left[\begin{array}{cc} c_1 + c_2 & -c_2 \\ & \\ -c_2 & c_2 \end{array}\right] \left[\begin{array}{c} \dot{\alpha}_1 \\ \\ \dot{\alpha}_2 \end{array}\right], \tag{26}$$

which has exactly the same form of the elastic stiffness matrix.

Equation (14) becomes therefore

$$\left[\mathbf{K} + \mathbf{G} - i\Omega\mathbf{C} - \Omega^2\mathbf{M}\right] \mathbf{a} = 0, \tag{27}$$

where the viscosity matrix $\mathbf{C}$ contains the c_i coefficients in equation (26) and the dynamics is governed by the nontrivial solutions of

$$\left[\begin{array}{cc} (\rho_1 y_1^2 + \rho_2 + 1)\lambda^2\omega^2 - 1 - k + i\omega(1+c)\epsilon + \eta & \lambda\,\omega^2(1 + \rho_2 y_2) + 1 - i\epsilon\omega \\ & \\ \lambda\,\omega^2(1 + \rho_2 y_2) + 1 - i\epsilon\omega & \omega^2(1 + \rho_2 y_2^2) - 1 + i\epsilon\omega + \eta/\lambda \end{array}\right] \left[\begin{array}{c} a_1 \\ \\ a_2 \end{array}\right] = 0, \tag{28}$$

where the following dimensionless constants have been introduced

$$c = \frac{c_1}{c_2}, \quad \epsilon = \frac{c_2}{l_2\sqrt{k_2 m_2}}. \tag{29}$$

The characteristic equation, obtained from the matrix (28) and written with the notation $\tilde{\omega} = -i\omega$, becomes

$$p_0\tilde{\omega}^4 + p_1\tilde{\omega}^3 + p_2\tilde{\omega}^2 + p_3\tilde{\omega} + p_4 = 0, \tag{30}$$

where

$$
\begin{aligned}
p_0 = {} & \lambda^2\left(\rho_2+\rho_1 y_1^2-\rho_2 y_2+\rho_2^2 y_2+\rho_1\rho_2 y_1^2 y_2-\rho_2^2 y_2^2\right),\\
p_1 = {} & \epsilon\left(1+c+2\lambda+\lambda^2+\lambda^2\rho_2+\lambda^2\rho_1 y_1^2+\rho_2 y_2\right.\\
& \left.\qquad +c\rho_2 y_2+2\lambda\rho_2 y_2\right),\\
p_2 = {} & 1+c\epsilon^2-\eta+k+\lambda\left[2-\eta+\lambda-(\eta-\lambda)\left(\rho_2+\rho_1 y_1^2\right)\right]\\
& \qquad +\rho_2 y_2\left(1-\eta+k+2\lambda\right),\\
p_3 = {} & \epsilon\left(c-\eta+k-\frac{\eta(1+c)}{\lambda}\right),\\
p_4 = {} & -\eta+k+\tfrac{\eta}{\lambda}\left(\eta-1-k\right).
\end{aligned}
\tag{31}
$$

Note that the notation $\tilde{\omega}=-i\omega$, corresponds to $\tilde{\Omega}=-i\Omega$, so that the time harmonic assumption, equation (12), becomes $\alpha_j=a_j\exp\tilde{\Omega}t$, and the instability occurs when $\mathrm{Re}[\tilde{\omega}]>0$.

A quasi-static solution of equation (30) corresponds to $\tilde{\omega}=0$ and can be found when $p_4=0$, which provides the two buckling loads (22). Therefore, the presence of the viscosity does not alter the quasi-static bifurcations of the double pendulum with dead load H; it will be shown that the situation changes when follower load are present.

2.3 The follower force P on the double pendulum

Assuming that the Ziegler double pendulum is loaded only with the follower force $\mathbf{P}$, so that $\mathbf{H}=0$, and using again the dimensionless variables (17), except that η is now replaced by

$$
\gamma=\frac{Pl_1}{k_2}, \tag{32}
$$

the generalized eigenvalue problem (13) can be compacted and leads to the condition of vanishing of the determinant of the matrix

$$
\left[\begin{array}{cc}
(\rho_1 y_1^2+\rho_2+1)\lambda^2\omega^2-1-k+\gamma & \lambda\,\omega^2(1+\rho_2 y_2)+1-\gamma\\
\lambda\,\omega^2(1+\rho_2 y_2)+1 & \omega^2(1+\rho_2 y_2^2)-1
\end{array}\right], \tag{33}
$$

a condition which immediately provides the two solutions for ω^2

$$\omega^2 = \frac{\beta_1 - \gamma\beta_2 \pm \sqrt{\left(\beta_1 - \gamma\beta_2\right)^2 - 4ka}}{2a}, \tag{34}$$

where a and β_1 are the same coefficients as in the list (21), again reported below to facilitate reading

$$\begin{aligned}
&a = \lambda^2 \left[y_1^2\rho_1 + (1-y_2)^2\rho_2 + y_1^2 y_2^2 \rho_1\rho_2\right] > 0,\\
&\beta_1 = \lambda \left[2 + 2y_2\rho_2 + \lambda(1 + y_1^2\rho_1 + \rho_2)\right] + (k+1)(1+\rho_2 y_2^2) > 0,\\
&\beta_2 = 1 + \lambda + y_2^2\rho_2 + y_2\lambda\rho_2 > 0.
\end{aligned} \tag{35}$$

From the pair of solutions (34) for ω^2, four solutions for Ω follow

$$\Omega = \pm\frac{1}{l_2}\sqrt{\frac{k_2}{m_2}}\sqrt{\frac{\beta_1 - \gamma\beta_2 \pm \sqrt{\left(\beta_1 - \gamma\beta_2\right)^2 - 4ka}}{2a}}. \tag{36}$$

Note that:

- It can be shown that both the the discriminant $\Delta = \left(\beta_1 - \gamma\beta_2\right)^2 - 4ka$ and the coefficient β_1 are strictly positive when $\gamma = 0$, in other words, $\Delta(0) > 0$ and $\beta_1(0) > 0$, so that all solutions Ω are real, which is coherent with the fact that the structure has to be stable when unloaded.
- For tensile load, $\gamma < 0$, all solutions Ω are real, which means that the structure is stable.
- As graphically represented in Fig. 3, the following conditions can be established:

$$\begin{aligned}
&\beta_1 - \gamma\beta_2 > 0 && \Longleftrightarrow \gamma < \frac{\beta_1}{\beta_2},\\
&\left(\beta_1 - \gamma\beta_2\right)^2 - 4ka < 0 && \Longleftrightarrow \frac{\beta_1}{\beta_2} - \frac{2\sqrt{k\,a}}{\beta_2}\\
& && \quad < \gamma < \frac{\beta_1}{\beta_2} + \frac{2\sqrt{k\,a}}{\beta_2}.
\end{aligned} \tag{37}$$

The following three possibilities only arise.

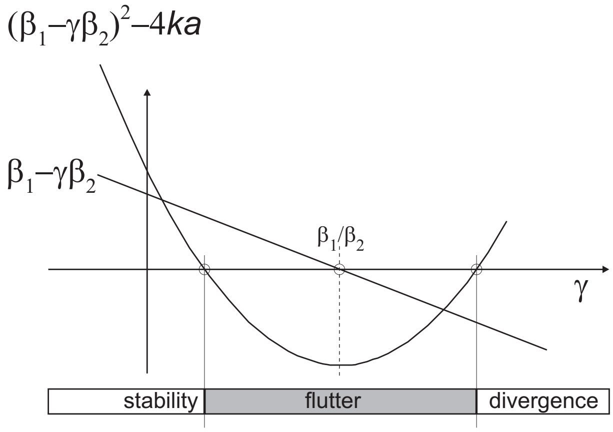

Figure 3. Graphical study of equation (34), showing a 'competition' between a linear $\beta_1 - \gamma\beta_2$ and a parabolic $(\beta_1 - \gamma\beta_2)^2 - 4ka$ term. Note that the magnitude of the follower load P is included in the variable γ, which determines the stability behaviour of the structure shown in Fig. 2 in the case $H = 0$.

- **Stability:** two real and positive values for ω^2, which correspond to four real Ω (two positive and two negative) and occur when $\gamma < \beta_1/\beta_2$ and $(\beta_1 - \gamma\beta_2)^2 - 4ka > 0$; vibrations are sinusoidal.
- **Flutter instability:** two complex conjugate values for ω^2, which correspond to two complex conjugate pairs for Ω and occur when $(\beta_1 - \gamma\beta_2)^2 - 4ka < 0$; four exponential solutions exist, namely, two unstable (which blow-up) and the other two decaying with time.
- **Divergence instability:** two real and negative values for ω^2, which correspond to two purely imaginary conjugate pairs for Ω and occur when $\gamma > \beta_1/\beta_2$ and $(\beta_1 - \gamma\beta_2)^2 - 4ka > 0$; vibrations become exponential functions of time, two of which amplify (denoting unstable behaviour) and two decay.

It should be noted that, while stability is always verified at sufficiently small load, flutter and divergence always occur when the load is sufficiently high, independently of the geometry and stiffness of the system. Moreover, flutter instability determines an interval of load separating stability from divergence.

As a conclusion, the response is *stable* when:

$$P < P_{flu}, \tag{38}$$

where

$$\frac{P_{flu} l_1}{k_2} = \frac{\lambda\left[2 + 2y_2\rho_2 + \lambda(1 + y_1^2\rho_1 + \rho_2)\right] + (k+1)(1 + \rho_2 y_2^2) - 2\sqrt{k\,a}}{1 + \lambda + y_2^2\rho_2 + y_2\lambda\rho_2}, \tag{39}$$

is the critical load for *flutter instability*, which occurs when the load P falls within the interval:

$$P_{flu} \le P < P_{div} \tag{40}$$

where

$$\frac{P_{div} l_1}{k_2} = \frac{\lambda\left[2 + 2y_2\rho_2 + \lambda(1 + y_1^2\rho_1 + \rho_2)\right] + (k+1)(1 + \rho_2 y_2^2) + 2\sqrt{k\,a}}{1 + \lambda + y_2^2\rho_2 + y_2\lambda\rho_2}, \tag{41}$$

is the critical load for *divergence instability*, which occurs for loads P higher than or equal to P_{div}.

Note that at the onset of flutter and divergence instabilities only two values of Ω are found from equation (36), both real and with opposite signs in the case of flutter, pure imaginary and with opposite signs in the case of divergence.

In the particular case in which there are only two masses, $m_3 = 0$, namely, $\rho_1 = \rho$, $\rho_2 = 0$, $y_1 = y$, the flutter load, equation (39), becomes

$$\frac{P_{flu} l_1}{k_2} = \frac{(1+\lambda)^2 + (\lambda y\sqrt{\rho} - \sqrt{k})^2}{1+\lambda}. \tag{42}$$

Therefore the load for flutter can be minimized in the situation where

$$\sqrt{k} = \lambda y \sqrt{\rho}, \quad \Longleftrightarrow \sqrt{\frac{k_1}{k_2}} = \frac{d}{l_2}\sqrt{\frac{m_1}{m_2}}, \tag{43}$$

which corresponds to

$$P_{flu} = k_2\left(\frac{1}{l_1} + \frac{1}{l_2}\right), \tag{44}$$

In CISM Lecture Notes No. 586 "Dynamic Stability and Bifurcation in Nonconservative Mechanics" (Ch. 1), edited by: D. Bigoni and O. Kirillov, Springer, ISBN 978-3-319-93721-2, doi 10.1007/978-3-319-93722-9

while the divergence load becomes

$$P_{div} = k_2 \left(\frac{1}{l_1} + \frac{1}{l_2} \right) + 4k_1 \frac{l_2}{l_1} \left(\frac{1}{l_1 + l_2} \right). \tag{45}$$

If it is assumed for simplicity $l_1 = l_2 = L$, $d = l_1$, $k_1 = k_2 = K$, and $m_1 = m_2$, the critical loads for flutter and divergence become simply

$$P_{flu} = 2\frac{K}{L}, \quad P_{div} = 4\frac{K}{L}. \tag{46}$$

It can finally be concluded that, in a linearized context, *while divergence instability corresponds to a motion growing exponentially in time, flutter instability corresponds to a blowing-up oscillation. Note that both these two instabilities cannot be detected with a quasi-static analysis.*

The above statement is confirmed in Fig. 4, where results are reported as numerical solution of the linear differential system (11) for $H = 0$ and with the initial conditions $\alpha_1 = \alpha_2 = 0.5°$ ($\alpha_1 = \alpha_2 = -0.5°$ for divergence) and $\dot{\alpha}_1 = \dot{\alpha}_2 = 0$. For the numerical solution, the following parameters (taken to be representative of the structural model that will be presented in Section 2.10) have been selected:

$$\begin{aligned} &l = 3\,d = 3\,h = 100\,mm, \quad m_1 = 12\,m_2 = 4\,m_3 = 552\,g, \\ &k_1 = k_2 = 0.189\,Nm, \end{aligned} \tag{47}$$

which correspond from equations (39) and (41) to a flutter load $P_{flu} \approx 4.8\,\mathrm{N}$ and to a divergence load $P_{div} \approx 8.8\,\mathrm{N}$, so that $P = 6.8\,\mathrm{N}$ ($P = 15.4\,\mathrm{N}$) has been assumed for the simulation of flutter (of divergence). A sequence 0.44 (0.2) seconds long of configurations at different instants of time is reported in Fig. 4, where each configuration is drawn at fixed intervals of time (0.04 s). The oscillatory blow-up (The exponential growth) of the solution is clearly visible in the case of flutter (of divergence).

Flutter cannot be detected via quasi-static bifurcation analysis Equation (42) shows that the flutter load for the Ziegler double pendulum with two masses, depends on the mass distribution of the system, through parameters y and ρ. This distribution, which does not influence the quasi-static behaviour, alters the load for flutter instability. In fact, if equation (42) is employed for the same set of parameters (stiffness and entity of masses) which yield the critical loads (46), but with a different *disposition of masses*, namely, $y_1 = d/l_1 = 1/2$ (instead than $y_1 = 1$), the following

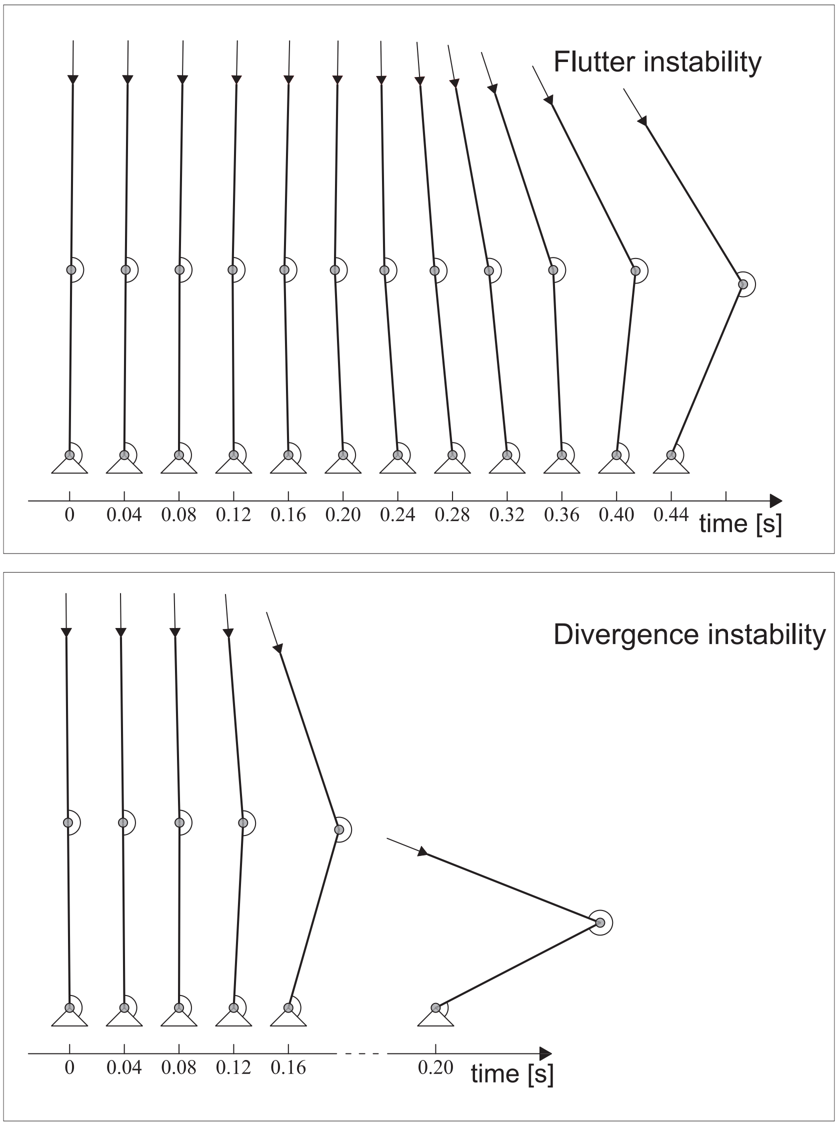

Figure 4. A sequence (0.44 s for flutter and to 0.2 s for divergence) of deformed configurations at consecutive time intervals of 0.04 seconds of the Ziegler double pendulum (sketched in Fig. 2 with $\mathbf{H} = 0$) and exhibiting flutter (upper part) and divergence (lower part) instability. Results have been obtained through a linearized analysis, equations (11), with initial conditions $\alpha_1 = \alpha_2 = 0.5°$ ($\alpha_1 = \alpha_2 = -0.5°$ for divergence) and $\dot{\alpha}_1 = \dot{\alpha}_2 = 0$, at the load $P = 6.8\,\mathrm{N}$ inside the flutter region (upper part) and at the load $P = 15.4\,\mathrm{N}$ inside the divergence region (lower part). The values of parameters employed for the analysis are reported in the list (47).

critical loads for flutter and divergence instability are obtained

$$P_{flu}(y_1 = 1/2) = \left(2 + \frac{1}{8}\right)\frac{K}{L}, \qquad P_{div}(y_1 = 1/2) = \frac{25}{8}\frac{K}{L}. \tag{48}$$

The fact that two different critical loads for flutter and divergence instability, namely, (46) and (48) are calculated for two mechanical systems differing only in the their mass distribution, which would not influence results calculated with the quasi-static criterion for bifurcation, shows that

the quasi-static criterion for bifurcation is inadequate to calculate critical loads of systems subject to follower loads.

2.4 Surprising effects related to the viscosity: the Ziegler paradox

The effect of viscosity on the flutter and divergence instability of the Ziegler double pendulum subject to the follower load P can be investigated by assuming that the two elastic hinges become viscoelastic, thus adding to equation (11) the term (26), to yield again equation (27), where now the geometric matrix $\mathbf{G}$ contains P. The dynamics of the double pendulum is governed by the nontrivial solution of

$$\begin{bmatrix} (\rho_1 y_1^2 + \rho_2 + 1)\lambda^2\omega^2 - 1 - k + i\omega(1+c)\epsilon + \gamma & \lambda\,\omega^2(1+\rho_2 y_2) + 1 - i\epsilon\omega - \gamma \\ \lambda\,\omega^2(1+\rho_2 y_2) + 1 - i\epsilon\omega & \omega^2(1+\rho_2 y_2^2) - 1 + i\epsilon\omega \end{bmatrix} \begin{bmatrix} a_1 \\ a_2 \end{bmatrix} = 0, \tag{49}$$

where the dimensionless constants (29) have been used.

Assuming for simplicity $l_1 = l_2 = L$, $k_1 = k_2 = K$, $\rho_1 = 1$, $\rho_2 = 0$, $y_1 = 1$, $\lambda = 1$, $k = 1$, $c = 1$, the problem (49) leads to the following characteristic equation

$$\det \begin{bmatrix} 2\omega^2 - 2 + 2i\epsilon\omega + \gamma & \omega^2 + 1 - i\epsilon\omega - \gamma \\ \omega^2 + 1 - i\epsilon\omega & \omega^2 - 1 + i\epsilon\omega \end{bmatrix} = 0, \tag{50}$$

which, written with the notation $\tilde{\omega} = -i\omega$, becomes

$$p_0\tilde{\omega}^4 + p_1\tilde{\omega}^3 + p_2\tilde{\omega}^2 + p_3\tilde{\omega} + p_4 = 0, \tag{51}$$

where

$$p_0 = 1, \quad p_1 = 6\epsilon, \quad p_2 = 6 + \epsilon^2 - 2\gamma, \quad p_3 = 2\epsilon, \quad p_4 = 1. \tag{52}$$

Note that the notation $\tilde{\omega} = -i\omega$, corresponds to $\tilde{\Omega} = -i\Omega$, so that the time harmonic assumption, equation (12), becomes $\alpha_j = a_j \exp \tilde{\Omega} t$, and the instability occurs when $\mathrm{Re}[\tilde{\omega}] > 0$ (divergence when $\mathrm{Im}[\tilde{\omega}] = 0$ and flutter when $\mathrm{Im}[\tilde{\omega}] \neq 0$). Note also that, differently from the case of dead loading, the characteristic equation (51) does not admit quasi-static solutions, $\tilde{\omega} = 0$, because p_4 cannot vanish.

The analysis of the nature of the solutions to the characteristic equation (51) can be performed using the Routh-Hurwitz criterion for a fourth-degree polynomial (see for instance Ziegler, 1977), so that *stability* is assured when

$$p_1 > 0, \quad p_1 p_2 - p_0 p_3 > 0, \quad (p_1 p_2 - p_3) p_3 - p_1^2 p_4 > 0, \quad p_4 > 0, \tag{53}$$

providing the following limit condition for stability

$$P^*_{flu} = \left(\frac{4}{3} + \frac{\epsilon^2}{2} \right) \frac{K}{L}. \tag{54}$$

The behaviour of the Ziegler double pendulum with viscoelastic hinges is shown in Fig. 5, where the real and imaginary parts of the eigenvalue $\tilde{\omega}$ are reported for three cases:

- The case in which the viscosity is absent 'from the beginning', which is governed by the characteristic equation provided by the determinant of the matrix (33);
- The viscoelastic case, which is governed by the characteristic equation (51) for two coefficients of viscosity, $\epsilon = 0.1$ and 0.5.

Fig. 5 shows that in the undamped case the real part of $\tilde{\omega}$ remains null, until the critical load for flutter (46) is reached, namely, $\gamma = 2$. After this value is met, the solution displays a positive real part, denoting an unstable character. The instability corresponds to flutter (and not to divergence) because, in addition to the positive real part, $\tilde{\omega}$ displays also an imaginary part. In the cases of viscoelastic hinges, the critical value for flutter decreases to $\gamma = 1.338$ (to $\gamma = 1.458$), for $\epsilon = 0.1$ (for $\epsilon = 0.5$). It should be noted that at decreasing viscosity the curves in the figure tend to the undamped case, but the critical load for flutter tends to that obtained from equation (54), in the limit of $\epsilon \to 0$, namely, $\gamma = 4/3 \approx 1.333$.

The critical load for flutter in the 'undamped system' (46), namely, in the case when the viscosity of the hinges is absent 'from the beginning', is notably higher than the value (54), so that a comparison between the flutter loads (46) and (54) leads to the following conclusions:

- the critical load for flutter is an increasing function of the viscosity parameter ϵ,
- *but this critical load at sufficiently small viscosity is smaller than the critical load calculated under the hypothesis that viscosity is absent*, so that for instance if $P_{flu} = 2K/L$ for the undamped system, P^*_{flu} decreases to $1.338K/L$ and $1.458K/L$ for ϵ equal to 0.1 and 0.5, respectively. Despite the fact that this behaviour is counter-intuitive, because adding an extra viscous 'constraint' to a system would apparently seem not lower a critical load, the conclusion is that *the introduction of a small viscosity in the Ziegler double pendulum reduces the critical load*;
- in the limit of vanishing viscosity, $\epsilon \to 0$, equation (54) yields $P^*_{flu} = 4/3\,K/L$, which does not coincide with (and is noticeably lower than) the flutter load for the undamped system (46), calculated for absent viscosity. This result is so surprising that it is known as 'the Ziegler paradox' and implies that *the flutter load calculated in the absence of viscosity is meaningless, as for a real structure some small, but never null, viscosity does always exist.*

The paradox was first discovered by Ziegler (1952), later framed in the general context of instability theory by Bottema (1956), and quoted by Bolotin (1963) as one of the most important theoretical aspects in stability when nonconservative forces are present. A modern and general discussion on the paradox can be found in (Kirillov, 2005, 2013). The destabilizing effect of viscous forces is now an accepted concept in mechanics and leads to the concept of 'dissipation instabilities' (Krechetnikov and Marsden, 2007; Kirillov and Verhulst, 2010, see also the chapter written by O. Doaré in the present book).

2.5 The deformation of an elastic rod: the Euler's elastica

The determination of the static and dynamic behaviour of an elastic *inextensible* rod subject to large deflection is a problem of great interest, which is here addressed in a two-dimensional context (in a reference system denoted through the two unit vectors $\mathbf{e}_1$ and $\mathbf{e}_2$). The purpose of this section is to provide the Euler elastica theory, including the case in which the material behaviour of the rod is viscoelastic and various external loadings are present, thus providing a generalization of Bigoni (2012) and Bigoni et al. (2015). Classical references are Love (1927), Reiss (1969), Audoly and Pomeau (2010).

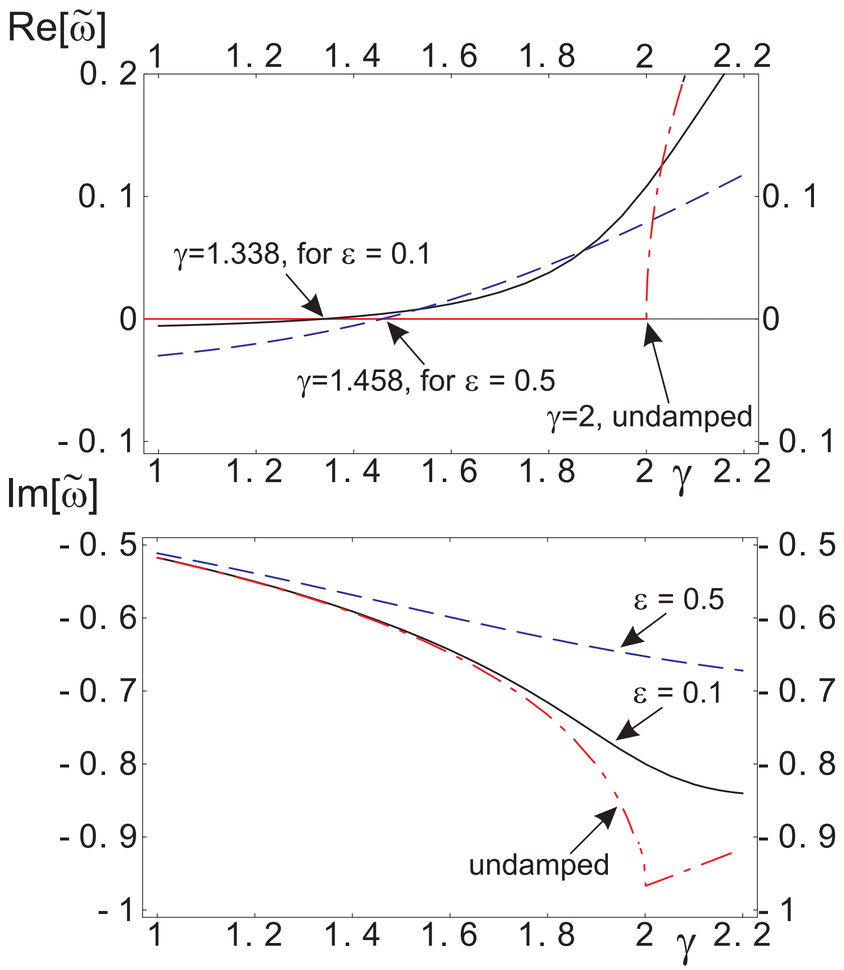

Figure 5. Behaviour (at varying the dimensionless load parameter γ) for the viscoelastic Ziegler double pendulum of the eigenvalue $\tilde{\omega}$, solved from equation (51). Two values, 0.1 and 0.5, of the viscosity dimensionless parameter ϵ are considered, together with the undamped case, where the viscosity is absent 'from the beginning'. The structure with $\epsilon = 0.1$ (with $\epsilon = 0.5$) suffers flutter instability at $\gamma = 1.338$ (at $\gamma = 1.458$), showing that the inclusion of viscosity lowers the flutter load from the value γ=2 obtained in the absence of viscosity. The Ziegler paradox is evident, because a vanishing small viscosity produces a drop in the flutter load from the value γ=2 of the undamped system, to $\gamma = 4/3$, corresponding to the damped system in the limit $\epsilon \to 0$.

In CISM Lecture Notes No. 586 "Dynamic Stability and Bifurcation in Nonconservative Mechanics" (Ch. 1), edited by: D. Bigoni and O. Kirillov, Springer, ISBN 978-3-319-93721-2, doi 10.1007/978-3-319-93722-9

Kinematics An *inextensible* rod of length l is considered, rectilinear in the reference configuration and smoothly deformed, as shown in Fig. 6. In the undeformed and deformed configurations, the generic point can be picked up using a coordinate $x_0 \in [0, l]$ in the reference configuration and a curvilinear coordinate $s \in [0, l]$ in the current configuration, so that inextensibility implies $x_0 = s$ and therefore $dx_0 = ds$.

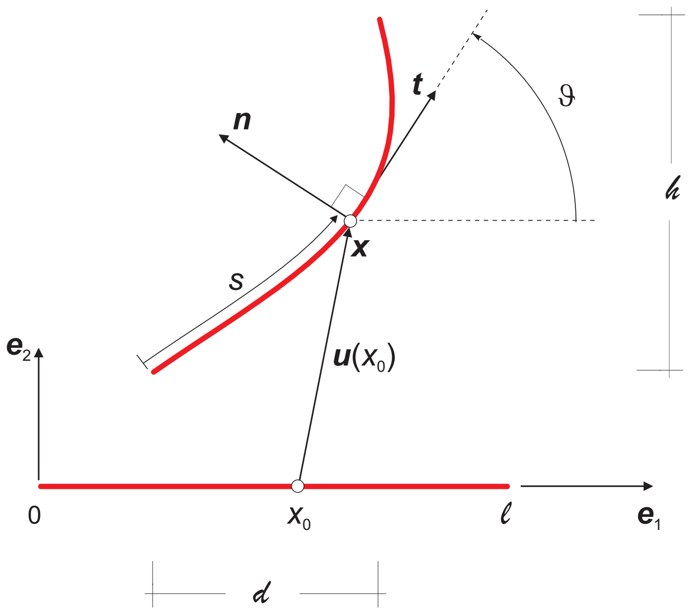

Figure 6. The kinematics of an elastic inextensible rod of length l, rectilinear in the reference configuration. Displacement of a point of coordinate x_0 is $\mathbf{u}(x_0) = \mathbf{x} - x_0\mathbf{e}_1$. Note that inextensibility implies that the curvilinear coordinate s is equal to the coordinate x_0, namely, $s = x_0$.

The *displacement* $\mathbf{u}$ of the point $x_0\mathbf{e}_1$ (where $\mathbf{e}_1$ is the unit vector singling out the axis of the undeformed rod) from the reference configuration is

$$\mathbf{u} = u_1(x_0)\mathbf{e}_1 + u_2(x_0)\mathbf{e}_2 = \mathbf{x} - x_0\mathbf{e}_1, \tag{55}$$

which, introducing the (twice-continuously differentiable) deformation

$$\mathbf{x} = \mathbf{g}(x_0), \tag{56}$$

becomes

$$\mathbf{u} = \mathbf{g}(x_0) - x_0\mathbf{e}_1. \tag{57}$$

Equation (56) is the parametric representation of the curve describing the elastica.

Two neighbor points are considered of the reference configuration at coordinates x_0 and $x_0 + \omega_0$, defining the vector $\mathbf{t}_0 = \omega_0 \mathbf{e}_1$. This vector is mapped to

$$\mathbf{g}(x_0 + \omega_0) - \mathbf{g}(x_0), \tag{58}$$

so that, assuming ω_0 small and performing a Taylor series expansion of the deformation around $\omega_0 = 0$, yields the transformed vector (tangent to the deformed line at x_0) as

$$\frac{\partial \mathbf{g}}{\partial x_0}\omega_0 = \left[\left(u_1' + 1\right)\mathbf{e}_1 + u_2' \mathbf{e}_2\right]\omega_0, \tag{59}$$

where the superscript $'$ denotes differentiation with respect to the coordinate $x_0 = s$.

Since the elastica is assumed *inextensible*, the transformed vector $\omega_0 \partial \mathbf{g}/\partial x_0$ must maintain the same length of the initial vector $\omega_0 \mathbf{e}_1$, a constraint which from equation (59) can be expressed as

$$\left|\frac{\partial \mathbf{g}}{\partial x_0}\right| = 1, \tag{60}$$

which, using equation (59) yields

$$u_1' + 1 = \operatorname{sgn}\left\{u_1' + 1\right\}\sqrt{1 - (u_2')^2}. \tag{61}$$

A derivative of equation (61) with respect to s, finally provides the inextensibility constraint in the form

$$u_1'' = -\operatorname{sgn}\left\{u_1' + 1\right\}\frac{u_2' u_2''}{\sqrt{1 - (u_2')^2}}. \tag{62}$$

Since the inextensibility constraint is enforced, the unit vector $\mathbf{t}$, tangent to the elastica at $\mathbf{x}$, is given by

$$\mathbf{t} = \left(u_1' + 1\right)\mathbf{e}_1 + u_2' \mathbf{e}_2 = \operatorname{sgn}\left\{u_1' + 1\right\}\sqrt{1 - (u_2')^2}\,\mathbf{e}_1 + u_2' \mathbf{e}_2, \tag{63}$$

and the angle θ of inclination of the tangent $\mathbf{t}$ to the elastica at $\mathbf{x}$ can be implicitly provided through the expressions

$$\sin\theta = x_2' = u_2', \quad \cos\theta = x_1' = u_1' + 1 = \operatorname{sgn}\left\{u_1' + 1\right\}\sqrt{1 - (u_2')^2}. \tag{64}$$

The signed length d of the projection of the elastica onto the $\mathbf{e}_1$ axis is

$$d = \int_0^l \cos\theta ds = l + u_1(l) - u_1(0) = \int_0^l \text{sgn}\left\{u_1' + 1\right\} \sqrt{1-(u_2')^2}\, ds, \quad (65)$$

while the signed projection onto the $\mathbf{e}_2$ axis is

$$h = \int_0^l \sin\theta ds = u_2(l) - u_2(0). \quad (66)$$

The unit vector $\mathbf{n}$ normal to the elastica at $\mathbf{x}$ can be obtained through differentiation (with respect to s) of the scalar product $\mathbf{t}\cdot\mathbf{t}$, so that $\mathbf{t}'$ is found to be orthogonal to $\mathbf{t}$ in the form

$$\begin{aligned} \mathbf{t}' &= -\text{sgn}\left\{u_1'+1\right\} \frac{u_2' u_2''}{\sqrt{1-(u_2')^2}}\mathbf{e}_1 + u_2''\mathbf{e}_2, \quad \text{or} \\ \mathbf{t}' &= -\theta' \sin\theta \mathbf{e}_1 + \theta' \cos\theta \mathbf{e}_2, \end{aligned} \quad (67)$$

and therefore the unit normal $\mathbf{n}$ can be obtained from equations $(67)_1$ or $(67)_2$, through division by the modulus $|\mathbf{t}'|$, which is the so-called 'curvature'

$$|\mathbf{t}'| = \frac{|u_2''|}{\sqrt{1-(u_2')^2}} = |\theta'|, \quad (68)$$

thus obtaining

$$\begin{aligned} \mathbf{n} &= \text{sgn}\left\{u_2''\right\} \left(-\text{sgn}\left\{u_1'+1\right\} u_2'\mathbf{e}_1 + \sqrt{1-(u_2')^2}\, \mathbf{e}_2\right) \quad \text{or,} \\ \mathbf{n} &= \text{sgn}\{\theta'\} \left(-\sin\theta \mathbf{e}_1 + \cos\theta \mathbf{e}_2\right). \end{aligned} \quad (69)$$

The *signed curvature* is

$$\theta' = \text{sgn}\left\{u_1'+1\right\} \frac{u_2''}{\sqrt{1-(u_2')^2}}, \quad (70)$$

Finally, the following unit vector $\mathbf{m}$ is introduced

$$\mathbf{m} = \sin\theta \mathbf{e}_1 - \cos\theta \mathbf{e}_2, \quad (71)$$

which is orthogonal to $\mathbf{t}$ and rotated of $\pi/2$ anticlockwise from it, so that it is always parallel to $\mathbf{n}$, but may differ in sign, and it satisfies the following relations

$$\mathbf{t}' = -\theta'\mathbf{m}, \qquad \mathbf{m}' = \theta'\mathbf{t}. \quad (72)$$

Force and internal action The elastica is subject to external forces and couples, which are assumed to be applied at points ('concentrated forces') or diffused along the line ('forces per unit length') of the elastica. It is also assumed that forces and moments are transmitted internally to the elastica, so that when this is ideally cut at a point and the internal forces given evidence, they represent the *internal action*, and provide the equilibrium of the rod, ideally separated into two parts, Fig. 7.

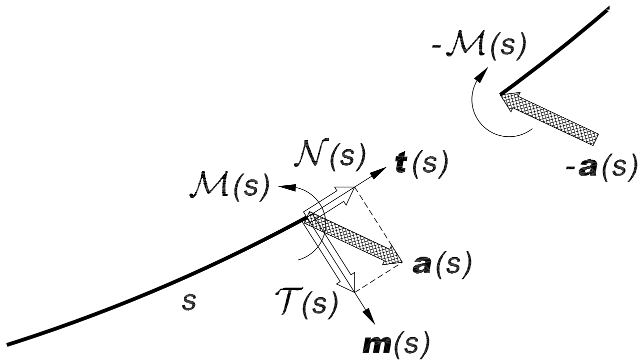

Figure 7. The action, force $\mathbf{a}(s)$ and moment $\mathcal{M}(s)$, internal to a deformed rod element. The Newton's law of action-reaction requires that if on the left side of the ideal cut, dividing the rod into two parts, the action is represented by the pair $\mathbf{a}(s)$ and $\mathcal{M}(s)$, on the right side the internal action becomes $-\mathbf{a}(s)$ and $-\mathcal{M}(s)$. The unit vectors $\mathbf{m}$ and $\mathbf{t}$ single out the normal and the tangential directions, respectively.

In the plane $\mathbf{e}_1$–$\mathbf{e}_2$ the internal action is comprised of a force $\mathbf{a}(s)$ and a moment vector $M(s)\mathbf{e}_3$, where $\mathbf{e}_3$ is the unit vector orthogonal to the plane. The figure 7 also shows that the internal action obeys the Newton's law of action-reaction, so that if on the left of the cut (characterized by the tangent vector $\mathbf{t}$ 'exiting' from the rod) the internal action is given by the pair $\mathbf{a}(s)$ and $\mathcal{M}(s)$, on the right hand (vector $\mathbf{t}$ 'entering' in the rod) the internal action is $-\mathbf{a}(s)$ and $-\mathcal{M}(s)$.

The internal force $\mathbf{a}$ is split into a normal, $\mathcal{N}(s)$, and a shear, $\mathcal{T}(s)$, component in the reference system $\mathbf{t}$ and $\mathbf{m}$ as

$$\mathbf{a}(s) = \mathcal{N}(s)\mathbf{t}(s) + \mathcal{T}(s)\mathbf{m}(s), \tag{73}$$

so that considering the equilibrium of a generic part of the rod free of concentrated forces, but subject to a generic distributed load $\mathbf{q}$, Fig. 8, the following conditions can be written down

$$
\begin{aligned}
&-\mathbf{a}(s_1)+\mathbf{a}(s_2)+\int_{s_1}^{s_2}\mathbf{q}(s)\,ds=0,\\
&\Big[\mathcal{M}(s)\mathbf{e}_3+[P(s)-O]\times\mathbf{a}(s)\Big]_{s_1}^{s_2}+\int_{s_1}^{s_2}[P(s)-O]\times\mathbf{q}(s)\,ds=0,
\end{aligned}
\tag{74}
$$

where $P(s)$ denotes a generic point on the elastica comprised between the two end points s_1 and s_2.

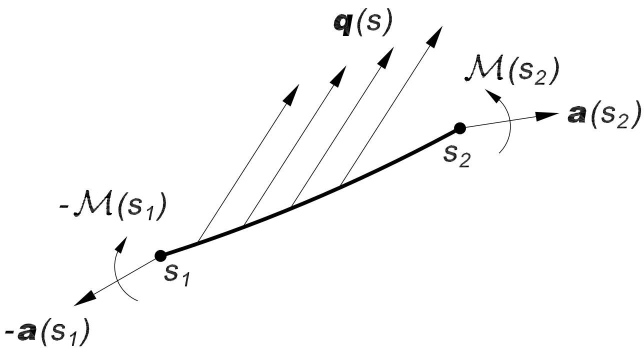

Figure 8. The equilibrium of a part of a deformed rod free of concentrated forces, but subject to a distributed load $\mathbf{q}$, defined per unit length. The internal action is represented through vector $\mathbf{a}(s)$ and moment $\mathcal{M}(s)$.

Since for every continuously differentiable function $f(s)$ the following identity holds true

$$
-f(s_1)+f(s_2)=\int_{s_1}^{s_2}f'(s)\,ds,
\tag{75}
$$

equation $(74)_1$ can be rewritten as

$$
\int_{s_1}^{s_2}\left[\mathbf{a}'(s)+\mathbf{q}\right]\,ds=0,
\tag{76}
$$

an equation which can be localized, because it holds true for every interval (s_1,s_2) free of concentrated forces, so that the following equation is obtained

$$
\mathbf{a}'(s)+\mathbf{q}=0.
\tag{77}
$$

On application again of the property (75) to equation $(74)_2$ yields

$$\int_{s_1}^{s_2} \left[\mathcal{M}'(s)\mathbf{e}_3 + P'(s) \times \mathbf{a}(s) + (P(s) - O) \times (\mathbf{a}'(s) + \mathbf{q}(s))\right] ds = 0, \quad (78)$$

where $P'(s) = \mathbf{t}$, so that equation (77) leads to the following condition

$$\int_{s_1}^{s_2} \left[\mathcal{M}'(s)\mathbf{e}_3 + \mathbf{t} \times \mathbf{a}(s)\right] ds = 0, \quad (79)$$

which can be localized and, keeping into account equation (73), provides

$$\mathcal{M}'(s) = \mathcal{T}(s). \quad (80)$$

The equations (77) and (80) are the equilibrium equations holding for the internal action along the rod. These equations can be written in components as

$$\begin{aligned} &\mathcal{N}' + \theta'\mathcal{T} + \mathbf{q} \cdot \mathbf{t} = 0, \\ &\mathcal{T}' - \theta'\mathcal{N} + \mathbf{q} \cdot \mathbf{m} = 0, \\ &\mathcal{M}'(s) = \mathcal{T}(s), \end{aligned} \quad (81)$$

which *hold true regardless the nature of the material of which the rod is made up.*

Finally, it can be noticed that equations $(81)_1$ and $(81)_3$ can be combined to obtain

$$\mathcal{N}' + \theta'\mathcal{M}' = -\mathbf{q} \cdot \mathbf{t}. \quad (82)$$

2.6 Constitutive equation and dynamics

For simplicity the elastica is assumed to be clamped at its left end, subject along the axis to forces per unit length of components q_1 and q_2 and to a load $\mathbf{P}$ (with components $-P_1$ and $-P_2$) at the other end (Fig. 9).

The *constitutive equation* used for the elastica is the following viscoelastic generalization of the Jacob Bernoulli's assumption that the deflection curvature is linearly proportional to the bending moment

$$\mathcal{M}(s) = B\theta'(s) + D\dot{\theta}'(s), \quad (83)$$

in which a superimposed dot denotes the time derivative, B is the bending stiffness, assumed constant for simplicity (in the linear beam theory B equals the product between the Young modulus of the rod and the moment of

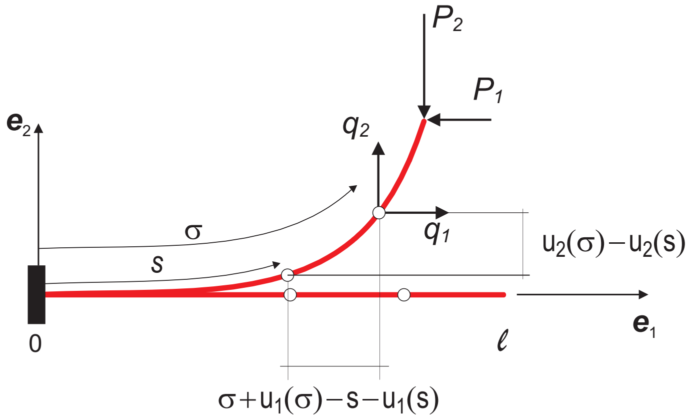

Figure 9. The clamped elastica subject to two forces P_1 and P_2 at the free end and to the forces per unit length q_1 and q_2.

inertia of its cross section), and D, assumed constant, accounts for the viscosity of the rod[4].

Note that for a purely elastic rod ($D = 0$) with constant bending stiffness B, a substitution of equation (83) into equation (82) provides the two equivalent conditions

$$\left(\mathcal{N} + B\frac{(\theta')^2}{2}\right)' = -\mathbf{q}\cdot\mathbf{t}, \qquad \left(\mathcal{N} + \frac{\mathcal{M}^2}{2B}\right)' = -\mathbf{q}\cdot\mathbf{t}. \tag{87}$$

With reference to two arbitrary points s and σ of the elastica, the following geometrical (thus holding for every constitutive equation of the rod)

[4] In a linearized theory, assuming for a rod a uniaxial $\sigma_1 - \epsilon_1$ constitutive law with an elastic term (singled out by the elastic modulus E) and a viscous term (characterized by a constant η) in the form

$$\sigma_1 = E\epsilon_1 + \eta\dot{\epsilon}_1, \tag{84}$$

the bending moment is given by

$$\mathcal{M} = \int_A \sigma_1 y\, dA = E\int_A \epsilon_1 y\, dA + \eta\int_A \dot{\epsilon}_1 y\, dA, \tag{85}$$

where A is the cross section of the rod and y is the position of a point measured orthogonally to the neutral axis. In a linearized theory $\epsilon = y\theta'$ and $\dot{\epsilon} = y\dot{\theta}'$, so that the bending moment becomes

$$\mathcal{M} = EI\theta' + \eta I\dot{\theta}', \tag{86}$$

where $I = \int_A y^2\, dA$ is the moment of inertia of the rod's transverse section.

relations can be written

$$u_2(\sigma)-u_2(s) = \int_s^\sigma \sin\theta(\xi)d\xi, \quad \sigma+u_1(\sigma)-s-u_1(s) = \int_s^\sigma \cos\theta(\xi)d\xi, \tag{88}$$

so that the bending moment at the generic point s can be calculated as generated by the following external loads

- (i.) the end force $\mathbf{P}$ of components $-P_1$ and $-P_2$,
- (ii.) the inertia force $-\rho\ddot{\mathbf{u}}$,
- (iii.) the external dissipative force $-\kappa\dot{\mathbf{u}}$ (defined per unit length of the rod, for instance the force generated by the air drag during vibrations),
- the diffused load $\mathbf{q}(s)$, with components q_1 and q_2,

in the form

$$\begin{aligned}\mathcal{M}(s) = \; & P_1\int_s^l \sin\theta(\sigma)d\sigma - P_2\int_s^l \cos\theta(\sigma)d\sigma \\ & -\int_s^l \Big(\rho\ddot{u}_2(\sigma)+\kappa\dot{u}_2(\sigma)-q_2(\sigma)\Big)\Big(\sigma+u_1(\sigma)-s-u_1(s)\Big)\,d\sigma \\ & +\int_s^l \Big(\rho\ddot{u}_1(\sigma)+\kappa\dot{u}_1(\sigma)-q_1(\sigma)\Big)\Big(u_2(\sigma)-u_2(s)\Big)\,d\sigma.\end{aligned} \tag{89}$$

Equating the 'external' moment (89) produced by the loads to the 'internal' moment generated by the curvature, equation (83), yields

$$\begin{aligned}& B\theta'(s)+D\dot{\theta}'(s)-P_1\int_s^l \sin\theta(\sigma)d\sigma + P_2\int_s^l \cos\theta(\sigma)d\sigma \\ & +\int_s^l \Big(\rho\ddot{u}_2(\sigma)+\kappa\dot{u}_2(\sigma)-q_2(\sigma)\Big)\Big(\sigma+u_1(\sigma)-s-u_1(s)\Big)\,d\sigma \\ & \qquad -\int_s^l \Big(\rho\ddot{u}_1(\sigma)+\kappa\dot{u}_1(\sigma)-q_1(\sigma)\Big)\Big(u_2(\sigma)-u_2(s)\Big)\,d\sigma = 0.\end{aligned} \tag{90}$$

A calculation of the first derivative of equation (90) with respect to s and use of equations (64) yields

$$\boxed{\begin{aligned}&\theta'' + \frac{D}{B}\dot{\theta}''(s)\\ &\qquad +\frac{1}{B}\left[P_1 + \int_s^l \Big(\rho\ddot{u}_1(\sigma) + \kappa\dot{u}_1(\sigma) - q_1(\sigma)\Big)\,d\sigma\right]\sin\theta(s)\\ &\qquad -\frac{1}{B}\left[P_2 + \int_s^l \Big(\rho\ddot{u}_2(\sigma) + \kappa\dot{u}_2(\sigma) - q_2(\sigma)\Big)\,d\sigma\right]\cos\theta(s) = 0,\end{aligned}} \tag{91}$$

which is the equation of the Euler's elastica, generalized to include (in addition to the two loads P_1 and P_2): internal viscosity (parameter D), external dissipation (parameter κ), external loading per unit length (parameter $\mathbf{q}$), inertial forces ($\rho\ddot{\mathbf{u}}$, where ρ is the mass density per unit length).

In the special case of a purely elastic rod $D = 0$, subject only to end loads P_1 and P_2, equation (91) reduces to the well-known form of the elastica (Bigoni, 2012; Bigoni et al., 2015)

$$\theta''(s) + \frac{P_1}{B}\sin\theta(s) - \frac{P_2}{B}\cos\theta(s) = 0. \tag{92}$$

Linearization. Assuming small oscillations about a rectilinear configuration, the rotation θ is small, so that equations (64) provide

$$u_2'(s) \approx \theta(s) \quad u_1'(s) \approx 0. \tag{93}$$

Equation $(93)_2$ implies that $u_1 = 0$ for the clamped rod and therefore equation (91) simplifies to

$$\begin{aligned}Bu_2'''(s) + D\dot{u}_2'''(s) + \left(P_1 - \int_s^l q_1(\sigma)\,d\sigma\right)u_2'(s)&\\ -P_2 - \int_s^l \Big(\rho\ddot{u}_2(\sigma) + \kappa\dot{u}_2(\sigma) - q_2(\sigma)\Big)\,d\sigma = 0,&\end{aligned} \tag{94}$$

which can be derived with respect to s to finally achieve the usual equation of the linearized theory (IV and roman numerals denote derivatives with respect to the variable x, which singles out points of the rod's axis)

$$\boxed{\begin{aligned}&Bu_2^{IV}(x) + D\dot{u}_2^{IV}(x) + \left(P_1 - \int_x^l q_1(\sigma)\,d\sigma\right)u_2^{II}(x) + q_1(x)u_2^{I}(x)\\ &\qquad\qquad +\rho\ddot{u}_2(x) + \kappa\dot{u}_2(x) - q_2(x) = 0,\end{aligned}} \tag{95}$$

In CISM Lecture Notes No. 586 "Dynamic Stability and Bifurcation in Nonconservative Mechanics" (Ch. 1), edited by: D. Bigoni and O. Kirillov, Springer, ISBN 978-3-319-93721-2, doi 10.1007/978-3-319-93722-9

Equation (95) governs the small vibrations of a straight viscoelastic rod of bending stiffness B and internal viscosity D, of mass ρ per unit length, prestressed with axial loads P_1 and q_1, subject to transverse load q_2 per unit length, and external viscosity κ (a simplified version of this equation is reported by Graff, 1975).

Boundary conditions

At the clamped end of the rod, $s = 0$, the following geometrical constraints have to be imposed:

$$u_1(0) = u_2(0) = 0, \qquad \theta(0) = 0, \tag{96}$$

while at the loaded end of the rod, $s = l$, the following conditions on the internal action hold:

$$\mathcal{N}(l) = \mathbf{P} \cdot \mathbf{t}(l), \qquad \mathcal{T}(l) = \mathbf{P} \cdot \mathbf{m}(l), \qquad \mathcal{M}(l) = 0, \tag{97}$$

where $\mathbf{P} = -P_1\mathbf{e}_1 - P_2\mathbf{e}_2$, so that

$$\begin{aligned} &\mathcal{N}(l) = -P_1 \cos\theta(l) - P_2 \sin\theta(l), \\ &\mathcal{T}(l) = -P_1 \sin\theta(l) + P_2 \cos\theta(l), \qquad \mathcal{M}(l) = 0. \end{aligned} \tag{98}$$

Linearization. Assuming small oscillations about a rectilinear configuration, the conditions (96) and (98) simplify to

$$\begin{aligned} &u_1(0) = u_2(0) = u_2'(0) = 0, \\ &\mathcal{N}(l) = -P_1 - P_2\theta(l), \qquad \mathcal{T}(l) = -P_1\theta(l) + P_2, \qquad \mathcal{M}(l) = 0. \end{aligned} \tag{99}$$

Note that in a linearized setting, the term $\mathcal{M}^2$ has to be disregarded in equation $(87)_2$, so that $\mathcal{N}' = \mathbf{q} \cdot \mathbf{t}$. Therefore, the linearized boundary conditions (99) are consistent with the internal action only if the term $P_2\theta(l)$ is negligible, so that $\mathcal{N}(l) = -P_1$. The term can be neglected for instance in the case of tangentially follower force, treated in the next Section, in fact in this case $P_2 = P \sin\theta(l) \approx P\theta(l)$, so that $\mathcal{N}(l) = -P_1 - P_2\theta^2(l) \approx -P_1$.

2.7 The Beck and Pflüger rods

Beck (1952) and Pflüger (1950, 1955) have introduced two schemes of cantilever rod, which are clamped at one end and subject to a tangential load at the other, Fig. 10. The Pflüger rod is a generalization of the Beck

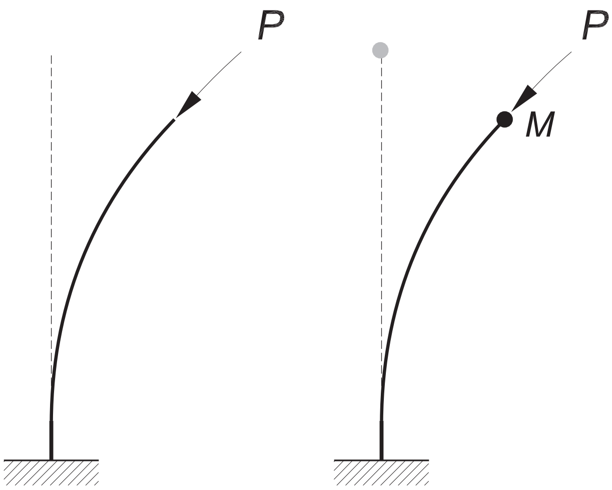

Figure 10. The Beck (left) and the Pflüger (right) rods. Note that the difference between the two structures is the presence in the latter of a concentrated mass M at its end.

rod, because in the former structure there is a concentrated mass positioned at the end where the tangential load is applied. These mechanical systems can be considered as the continuous elastic realization of the Ziegler double pendulum.

It should be noted that non-trivial static equilibrium, where $\dot{\theta} = 0$, can be shown to be impossible for both the Beck and Pflüger rods, regardless the magnitude of displacements (but for deformed configurations in which the normal force inside the rod remains compressive). In fact, equation $(87)_2$, valid for $D = 0$ or $\dot{\theta} = 0$, in the absence of tangential diffuse load, $\mathbf{q} \cdot \mathbf{t} = 0$, implies

$$\mathcal{N} + \frac{\mathcal{M}^2}{2B} = constant, \tag{100}$$

so that, since $\mathcal{M} = 0$ and $\mathcal{N} = -P$ at the loaded end of the rod, the condition

$$\mathcal{N} + \frac{\mathcal{M}^2}{2B} = -P, \tag{101}$$

has to hold true along the axis of the Beck and Pflüger rods in a static solution. The condition (101) can only be satisfied in the rectilinear configuration, because $\mathcal{M}^2 \geq 0$ and $|\mathcal{N}| \leq |P|$, so that only the undeformed configuration is a possible static solution.

In CISM Lecture Notes No. 586 "Dynamic Stability and Bifurcation in Nonconservative Mechanics" (Ch. 1), edited by: D. Bigoni and O. Kirillov, Springer, ISBN 978-3-319-93721-2, doi 10.1007/978-3-319-93722-9

Linearized analysis of the Pflüger rod

Denoting the rod's deflection u_2 as $-v$ (so that the transverse displacement is positive when opposite to $\mathbf{e}_2$), equation (95) governs the linearized dynamics of a straight rod, in which the relation $\theta(x) = -v^I(x)$ holds true. The moment-curvature viscoelastic constitutive relation (83) becomes now

$$\mathcal{M}(x,t) = -Bv^{II}(x,t) - D\dot{v}^{II}(x,t), \tag{102}$$

where a superimposed dot denotes the time derivative. The shear force $\mathcal{T}(x)$ can be computed from equation $(81)_3$ to be the derivative of the bending moment, so that, for constants moduli B and D, it can be written as

$$\mathcal{T}(x,t) = -Bv^{III}(x,t) - D\dot{v}^{III}(x,t). \tag{103}$$

For the Pflüger column of length l with a concentrated mass M (rotational inertia of the mass is neglected), the boundary conditions can easily be deduced from equations (99) and are

$$\begin{aligned}
&v(0,t) = v^I(0,t) = 0, && \text{clamped end,}\\
&\mathcal{M}(l,t) = -Bv^{II}(l,t) - D\dot{v}^{II}(l,t) = 0, && \text{loaded end,}\\
&\mathcal{T}(l,t) = -Bv^{III}(l,t) - D\dot{v}^{III}(l,t) = -M\ddot{v}(l,t), && \text{loaded end.}
\end{aligned} \tag{104}$$

The linearized differential equation of motion (95) which governs the dynamics of a rod subject to small displacements, to an an axial force P (positive when compressive), and to a distributed external damping κ is

$$Bv^{IV}(x,t) + D\dot{v}^{IV}(x,t) + Pv^{II}(x,t) + \kappa\dot{v}(x,t) + \rho\ddot{v}(x,t) = 0, \tag{105}$$

which, introducing the dimensionless quantities

$$\begin{aligned}
&\xi = \frac{x}{l},\ \tau = \frac{t}{l^2}\sqrt{\frac{B}{\rho}},\ p = \frac{Pl^2}{B},\ \alpha = \arctan\left(\frac{M}{\rho l}\right),\\
&\eta = \frac{D}{Bl^2}\sqrt{\frac{B}{\rho}},\ \gamma = \frac{\kappa l^2}{\sqrt{\rho B}},
\end{aligned} \tag{106}$$

can be rewritten as

$$v^{IV}(\xi,\tau) + \eta\dot{v}^{IV}(\xi,\tau) + pv^{II}(\xi,\tau) + \gamma\dot{v}(\xi,\tau) + \ddot{v}(\xi,\tau) = 0, \tag{107}$$

where now a roman numeral denotes differentiation with respect to ξ and a dot differentiation with respect to τ.

Governing equations Assuming time-harmonic vibrations of pulsation $\tilde{\omega}$

$$v(\xi, \tau) = \tilde{v}(\xi) e^{\tilde{\omega}\tau}, \tag{108}$$

equation (107) yields a linear differential equation for $\tilde{v}(\xi)$, which can be written as

$$\mathcal{L}[\tilde{v}] = -\tilde{\omega}^2 \tilde{v}, \tag{109}$$

where the differential operator $\mathcal{L}$ is defined as

$$\mathcal{L}[Y] = (1 + \tilde{\omega}\eta) \frac{d^4 Y}{d\xi^4} + p \frac{d^2 Y}{d\xi^2} + \tilde{\omega}\gamma Y, \tag{110}$$

and has to be complemented by the boundary conditions (104) now rewritten as

$$\begin{aligned} &\tilde{v}(0) = \tilde{v}'(0) = 0, && \text{clamped end,} \\ &\tilde{v}''(1) = 0, && \text{loaded end,} \\ &(1 + \eta\tilde{\omega})\tilde{v}'''(1) - \tilde{\omega}^2 \tan(\alpha)\tilde{v}(1) = 0, && \text{loaded end.} \end{aligned} \tag{111}$$

The differential problem (109) with the boundary conditions (111) always admits the trivial solution $\tilde{v} = 0$.

The characteristic equation of the differential equation (109) is

$$\lambda^4(1 + \eta\tilde{\omega}) + \lambda^2 p + \gamma\tilde{\omega} + \tilde{\omega}^2 = 0, \tag{112}$$

which admits the two solutions for λ^2

$$\lambda_{1,2}^2 = \frac{-p \pm \sqrt{p^2 - 4(1 + \eta\tilde{\omega})(\gamma\tilde{\omega} + \tilde{\omega}^2)}}{2(1 + \eta\tilde{\omega})}. \tag{113}$$

Therefore, the solution for $\tilde{v}$ becomes

$$\tilde{v}(\xi) = A_1 \sinh(\lambda_1 \xi) + A_2 \cosh(\lambda_1 \xi) + A_3 \sin(\lambda_2 \xi) + A_4 \cos(\lambda_2 \xi), \tag{114}$$

where A_i $(i = 1, .., 4)$ are arbitrary constants.

A substitution of the solution (114) into the boundary conditions (111) yields an algebraic system of equations which admits non-trivial solutions at the vanishing of the matrix of coefficients

$$\begin{bmatrix} 0 & 1 & 0 & 1 \\ \lambda_1 & 0 & \lambda_2 & 0 \\ \lambda_1^2 \sinh\lambda_1 & \lambda_1^2 \cosh\lambda_1 & -\lambda_2^2 \sin\lambda_2 & -\lambda_2^2 \cos\lambda_2 \\ a_{41} & a_{42} & a_{43} & a_{44} \end{bmatrix} \tag{115}$$

where

$$\begin{aligned}
a_{41} &= (1+\eta\tilde{\omega})\lambda_1^3\cosh\lambda_1 - \tilde{\omega}^2\tan\alpha\sinh\lambda_1,\\
a_{42} &= (1+\eta\tilde{\omega})\lambda_1^3\sinh\lambda_1 - \tilde{\omega}^2\tan\alpha\cosh\lambda_1,\\
a_{43} &= -(1+\eta\tilde{\omega})\lambda_2^3\cos\lambda_2 - \tilde{\omega}^2\tan\alpha\sin\lambda_2,\\
a_{44} &= (1+\eta\tilde{\omega})\lambda_2^3\sin\lambda_2 - \tilde{\omega}^2\tan\alpha\cos\lambda_2.
\end{aligned} \tag{116}$$

Noting that the λ_i's are functions of the applied load p, the pulsation $\tilde{\omega}$, the viscosity η, and the damping γ, nontrivial solutions for the vibrations of the Pflüger rod correspond to the fulfillment of the condition

$$f(p,\tilde{\omega},\alpha,\gamma,\eta) = 0, \tag{117}$$

where

$$\begin{aligned}
f(p,\tilde{\omega},\alpha,\gamma,\eta) \quad &= (1+\eta\tilde{\omega})(\lambda_1^4+\lambda_2^4)\\
&+2(1+\eta\tilde{\omega})\lambda_1^2\lambda_2^2\cosh\lambda_1\cos\lambda_2\\
&+\lambda_1\lambda_2(1+\eta\tilde{\omega})(\lambda_2^2-\lambda_1^2)\sinh\lambda_1\sin\lambda_2\\
&-\tilde{\omega}^2\tan\alpha\frac{\lambda_1^2+\lambda_2^2}{\lambda_1\lambda_2}[\lambda_2\sinh\lambda_1\cos\lambda_2\\
&-\lambda_1\cosh\lambda_1\sin\lambda_2].
\end{aligned} \tag{118}$$

For a given elastic system, the dimensionless parameters α, γ, and η are fixed. Therefore, for a fixed value of the dimensionless load p, equation (117) can be solved for $\tilde{\omega}$. If the real part of $\tilde{\omega}$ is positive, the system is unstable and in this case, if $\tilde{\omega}$ has also a complex part, *flutter instability* occurs, otherwise *divergence instability* occurs.

Note that both flutter instability and divergence instability occur for the Pflüger column (the former is achieved at critical loads smaller than those inducing the latter), except in the limit case of the Beck column ($\alpha = 0$), where the divergence load tends to infinity and it is therefore not found.

An example of determination of flutter instability for the Beck column in the presence of internal damping, but not external, is reported in Fig.

11, where the following values of parameters have been used:

$$\begin{aligned}
&l = 0.350 \text{ m}, \qquad \rho = 0.0546 \text{ kg/m}, \qquad B = 0.0332 \text{ Nm}^2, \\
&D = 7.078 \times 10^{-6} \text{ Nsm}^2, \qquad P = 5.5 \text{ N}.
\end{aligned} \tag{119}$$

The branches of the real ($\mathrm{Re}[\tilde{\omega}]$) and imaginary ($\mathrm{Im}[\tilde{\omega}]$) parts of the pulsation for vibration of the Beck column are reported in Fig. 11 as functions of the dimensionless load p.

The undamped case (in which damping is absent 'from the beginning') is reported on the upper part of Fig. 11, where flutter occurs at $p = 20.05$ a value found by Beck (1952), which is much higher than the value (2.467) associated with Euler's buckling of the same structure subject to dead loading. For the Beck's column divergence is not found. The case in which the only dissipation source is the internal damping is shown on the lower part, where the flutter load decreases to $p = 10.94$. Flutter occurs when a real branch of the pulsation $\tilde{\omega}$ becomes positive (with non-null values of its imaginary part). This figure shows clearly the strong detrimental effect of dissipation on the flutter critical load, which decreases from $p = 20.05$ to $p = 10.94$.

An example of determination of flutter for the Pflüger column in the presence of internal damping, but not external, is reported in Fig. 12, where, in addition to the values of the parameter list (119), $M/(\rho l) = 1$ has been assumed, so that $\tan\alpha = 1$.

The most important difference between results reported in Fig. 11 and Fig. 12 is that for the Pflüger column divergence instability also occurs in addition to flutter, so that the two critical loads for these instabilities determine the flutter region. In the undamped case (where damping is not introduced) the critical loads for flutter and divergence are respectively $p = 16.51$ and $p = 30.22$ (on the upper part of Fig. 12), which become $p = 7.78$ and $p = 30.52$ when internal damping is present (on the lower part of Fig. 12).

It can be therefore concluded that the presence of internal damping increases the size of the flutter region by strongly decreasing the flutter load and by slightly increasing the divergence load.

It is finally noticed that rotary damping (in other words a damping connected to the rotation of the rod's cross section) has also been considered, the interested reader is addressed to (Lottati and Elishakoff, 1987).

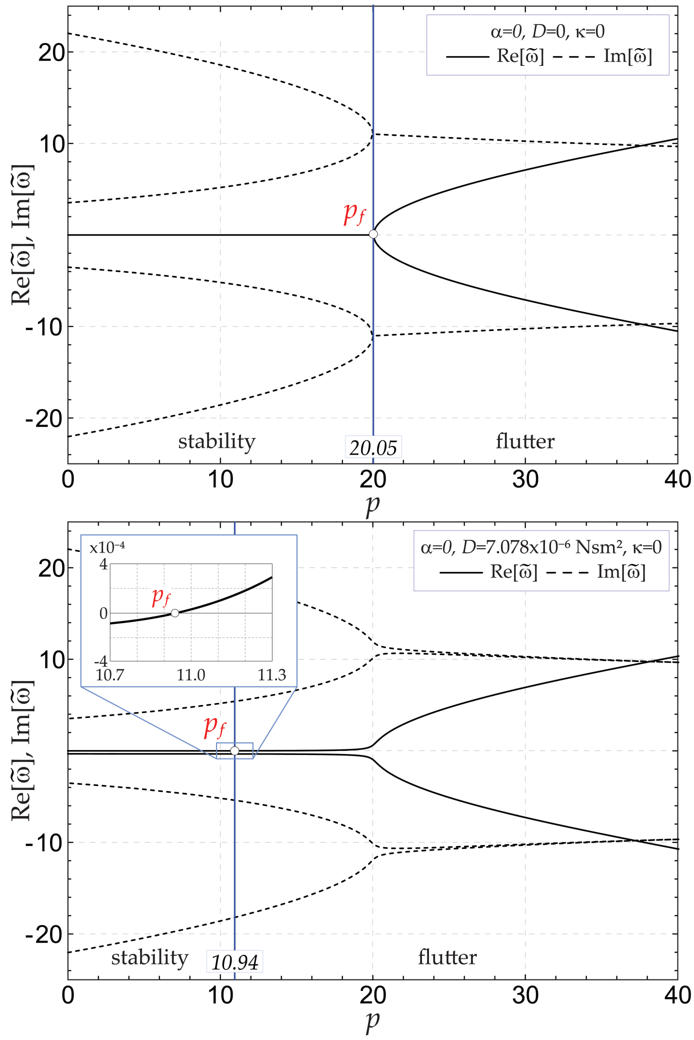

Figure 11. Branches of the real (Re[$\tilde{\omega}$]) and imaginary (Im[$\tilde{\omega}$]) parts of the pulsation for vibration of the Beck column as functions of the dimensionless load p. The undamped case (in which damping is absent 'from the beginning') is reported on the upper part, where flutter occurs at $p = 20.05$. The case in which internal damping is present (but there is no external damping) is shown on the lower part. Here, the flutter load decreases to $p = 10.94$. Flutter occurs when a real branch of the pulsation $\tilde{\omega}$ becomes positive (with non-null values of its imaginary part). Note the detrimental effect of dissipation on the critical load for flutter.

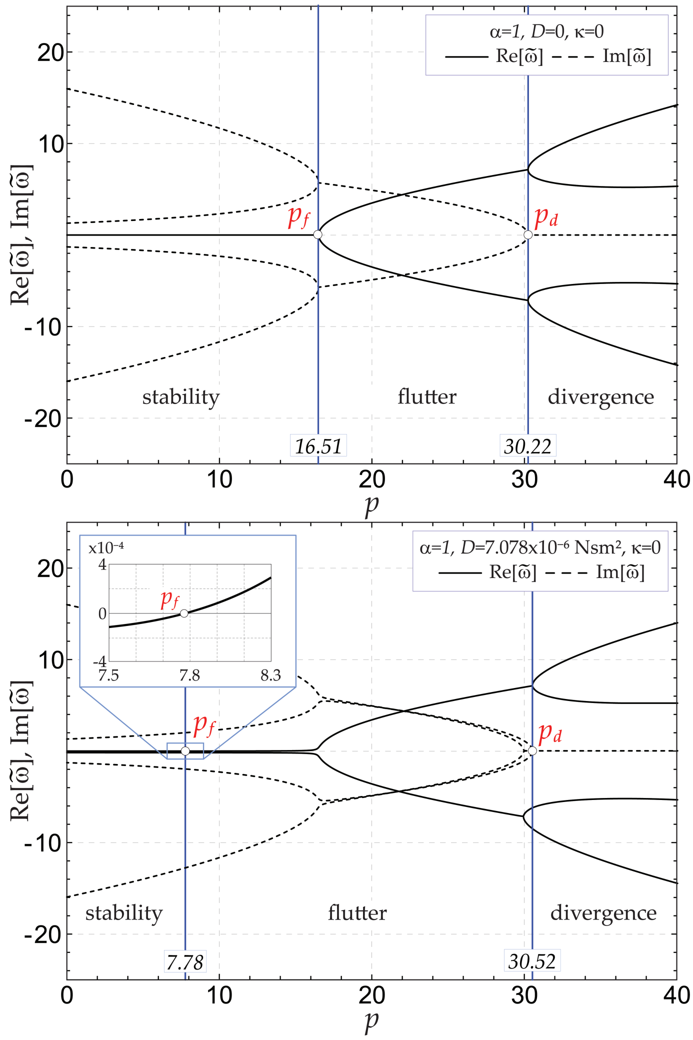

Figure 12. Branches of the real ($\mathrm{Re}[\tilde{\omega}]$) and imaginary ($\mathrm{Im}[\tilde{\omega}]$) parts of the pulsation for vibration of the Pflüger column (with $\tan\alpha = M/(\rho l) = 1$) as functions of the dimensionless load p. The undamped case (in which damping is absent 'from the beginning') is reported on the upper part, where flutter (marked with the subscript f) occurs at $p = 16.51$ and divergence (marked with the subscript d) at $p = 30.22$. The case in which internal damping is present (but there is no external damping) is shown on the lower part. Here, the flutter load decreases to $p = 7.78$, while the divergence load increases to $p = 30.52$. The flutter load strongly decreases with the introduction of the internal viscosity, while the divergence load slightly increases.

2.8 Self-adjointness, an exclusion condition for flutter

For discrete systems, unsymmetry of the geometric matrix in equation (11) is a necessary condition for flutter instability, which is in fact impossible for dead loading, ruled by a symmetric matrix. It is important now to obtain a condition similar to symmetry for discrete systems, which excludes flutter instability for continuous systems.

It is assumed, for simplicity, a null internal and external viscosity, $\eta = \gamma = 0$, and the Beck rod (where $\alpha = 0$) is considered. Moreover, for comparison, the 'standard' case of dead loading is also treated.

In both cases of follower and dead load, the differential operator is the same, which is the following reduction of the operator (110),

$$\mathcal{L}[Y] = \frac{d^4 Y}{d\xi^4} + p\frac{d^2 Y}{d\xi^2}, \tag{120}$$

so that the differential equation (109), complemented with the boundary conditions

$$\begin{aligned}
&\tilde{v}(0) = \tilde{v}^I(0) = 0, && \text{clamped end,}\\
&\tilde{v}^{II}(1) = 0, && \text{loaded end,}\\
&\tilde{v}^{III}(1) = \begin{cases} 0, & \text{loaded end for follower load,}\\ -p\tilde{v}^I(1), & \text{loaded end for dead load,}\end{cases}
\end{aligned} \tag{121}$$

becomes a Sturm-Liouville problem (Broman, 1970) for a fourth-order differential equation (note that the only difference between dead and follower load is in the boundary condition involving the shear force). For this differential problem *self-adjointness* excludes complex eigenvalues $\tilde{\omega}^2$, so that flutter instability is a-priori ruled out.

The condition of *self-adjointness (or symmetry) of the differential operator* $\mathcal{L}$ [defined by equation (120)] is

$$\int_0^1 \mathcal{L}[Y(\xi)]X(\xi)\, d\xi = \int_0^1 \mathcal{L}[X(\xi)]Y(\xi)\, d\xi, \tag{122}$$

which has to hold for every pair of functions $X(\xi)$ and $Y(\xi)$, both satisfying the boundary conditions (121).

A repeated use of integration by parts, namely,

$$\begin{aligned}
Y^{IV}X = \;& \left(Y^{III}X\right)^I - \left(Y^{II}X^I\right)^I + \left(Y^I X^{II}\right)^I\\
& - \left(YX^{III}\right)^I + YX^{IV},\\
Y^{II}X = \;& \left(Y^I X\right)^I - \left(YX^I\right)^I + YX^{II},
\end{aligned} \tag{123}$$

allows to obtain the following identity

$$
\begin{aligned}
\int_0^1 \mathcal{L}[Y(\xi)]X(\xi)\,d\xi = & \int_0^1 \mathcal{L}[X(\xi)]Y(\xi)\,d\xi \\
+ & \; p\left(Y^I X - Y X^I\right)_0^1 \\
+ & \left(Y^{III} X - Y^{II} X^I + Y^I X^{II} - Y X^{III}\right)_0^1,
\end{aligned}
\tag{124}
$$

which makes evident that the self-adjointness condition (122) involves the boundary conditions and is equivalent (for the problem under consideration) to

$$
\left(Y^{III} X - Y^{II} X^I + Y^I X^{II} - Y X^{III}\right)_0^1 + p\left(Y^I X - Y X^I\right)_0^1 = 0. \tag{125}
$$

Imposition of the boundary conditions $(121)_{1,2}$ at the clamp and the null moment condition at the loaded end $(121)_3$ yields the following self-adjointness condition

$$
Y^{III}(1)X(1) - Y(1)X^{III}(1) + p\left(Y^I(1)X(1) - Y(1)X^I(1)\right) = 0, \tag{126}
$$

valid for both the structures subject to the follower load and to the dead load, because the two structures differ only in the boundary condition on shear, equation $(121)_4$.

A consideration of the boundary condition $(121)_4$ shows that the self-adjointness condition (126) is *satisfied for dead loading*, in which case flutter instability is excluded, but is *not satisfied for follower load*, so that flutter instability becomes possible in that case.

2.9 Beyond the linearized solution: limit cycle behaviour

The stability analysis developed so far for the Beck and Pflüger columns is based on the time-harmonic solution, which is valid for the *linearized equations of motion* (95). This analysis is valid therefore only in a neighborhood of the instability point, but neglecting nonlinear terms becomes unacceptable when the motion starts to grow.

For the Ziegler double pendulum, the linearized problem is governed by equations (11) and the nonlinear dynamics by the equations (10), which can be integrated in time to provide the behaviour of the Ziegler double pendulum in the flutter and divergence regions, where large displacements and rotations are allowed. This integration has been numerically performed (using the function NDSolve of Mathematica 10.0) for the following values of constants:

$l_1 = l_2 = 0.1\,\text{m}$, $k_1 = k_2 = 0.189\,\text{Nm}$, $c_1 = c_2 = 0.006\,\text{Nms}$,
$m_1 = m_2 = 0.2\,\text{Kg}$, $m_3 = 0$, $d = l_1$, $P = 1.5\,P^*_{flu}$,

with P^*_{flu} evaluated through equation (54) and an initial imperfection $\alpha_1 = \alpha_2 = 0.1°$.

Numerical integration leads to the trajectory plotted in the phase plane reported in Fig. 13. It is clear from Fig. 13 and from Fig. 14, which

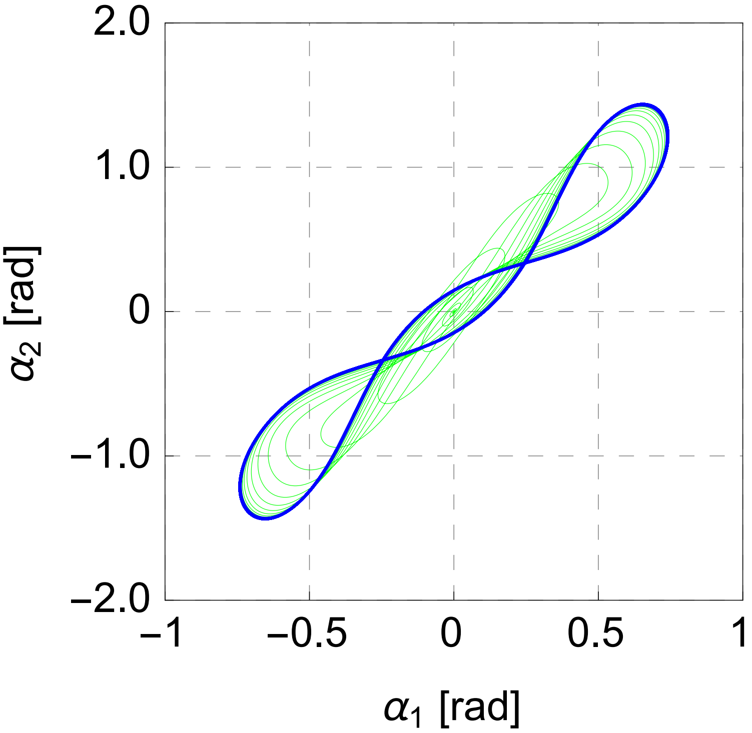

Figure 13. Trajectory in the α_1–α_2 phase plane for the Ziegler double pendulum (with viscoelastic hinges), which attains a stable limit cycle.

completes the phase portrait by showing the angular velocities $\dot{\alpha}_1$ and $\dot{\alpha}_2$ (plotted as functions of the rotations α_1 and α_2), that the Ziegler double pendulum reaches a stable limit cycle (see also D'Annibale et al., 2015).

When the structure reaches a limit cycle, self-sustained vibrations occur and the system behaves as a self-oscillating structure (Jenkins, 2013). The attainment of a limit cycle is a consequence of the dissipation, which is represented by the viscosity of the hinges for the Ziegler double pendulum.

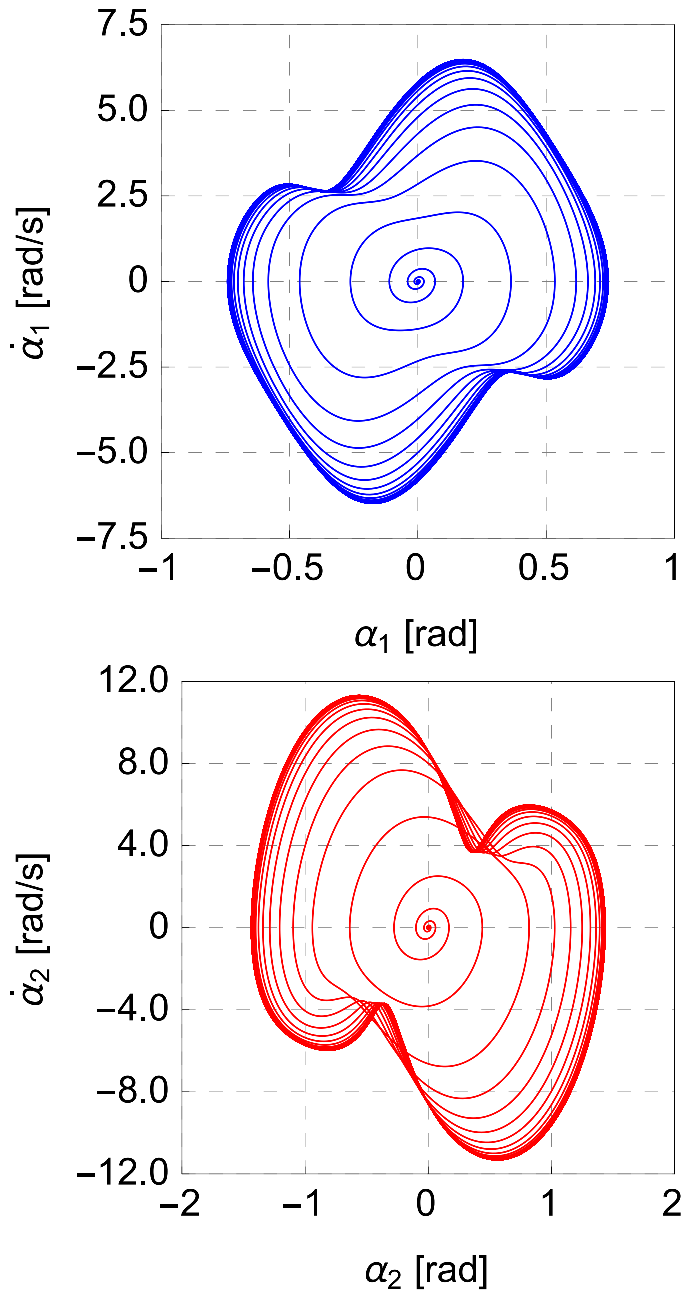

Figure 14. Angular velocities $\dot{\alpha}_1$ (upper part) and $\dot{\alpha}_2$ (lower part) as functions of the rotations α_1 and α_2, completing the phase portrait (see also Fig. 13), of the Ziegler double pendulum (with viscoelastic hinges), which reaches a stable limit cycle.

For the Beck's column in the absence of external damping, but in the presence of internal damping, Fig. 15, shows the trajectory of the end of the rod, while Fig. 16 and Fig. 17 complete the phase portrait by reporting the velocities of the end of the rod, plotted, respectively, as functions of the displacement components and in a $\dot{u}_1$–$\dot{u}_2$ representation. Values from the list (119) of parameters have been used.

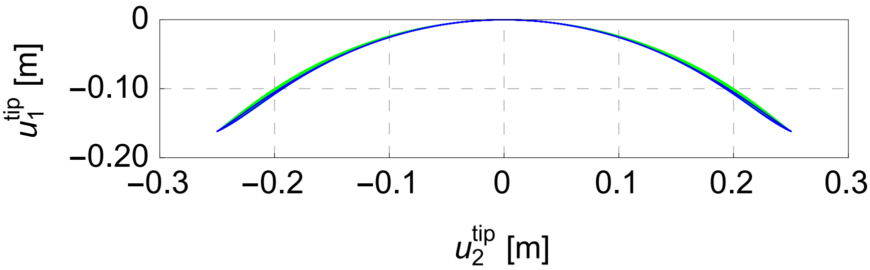

Figure 15. Trajectory of the loaded end of the Beck's column (the displacement components u_1^{tip} and u_2^{tip} of the rod's end are reported) with internal, but not external, dissipation, showing the achievement of a limit cycle. Note that this limit cycle is a closed loop, which is rather flat and therefore hardly visible.

Figs. 15–17 have been obtained with a nonlinear computational model, implemented in the finite element software ABAQUS Standard 6.13-2. Specifically, 2-nodes linear elements of type B21 (in the ABAQUS nomenclature) were employed to discretize the viscoelastic rod of constant, rectangular cross section. A number of 20 elements was found to be sufficient to adequately resolve for the rod dynamics. A linear viscoelastic model of the Kelvin-Voigt type was implemented for the constitutive response of the rod by means of a UMAT user subroutine, such that the bending moment was proportional to the rod curvature and its time derivative respectively through the elastic and viscous moduli. In the analysis, a rod of length l = 0.35 m, B = 0.0332 Nm^2, D = 7.078×10-6 Nsm^2, and density ρ = 0.0546 kg/m was subject at its tip to a tangential follower force P = 5.5 N (inside the flutter region). The dynamic analysis was performed by exploiting the default settings of ABAQUS Standard 6.13-2 and with a time increment of 10-4 seconds.

Figs. 15–17 suggest that the Beck's column reaches a limit cycle, even if the attainment of this limit cycle has not been formally proven, because the system has infinite degrees of freedom and only a numerical analysis was performed.

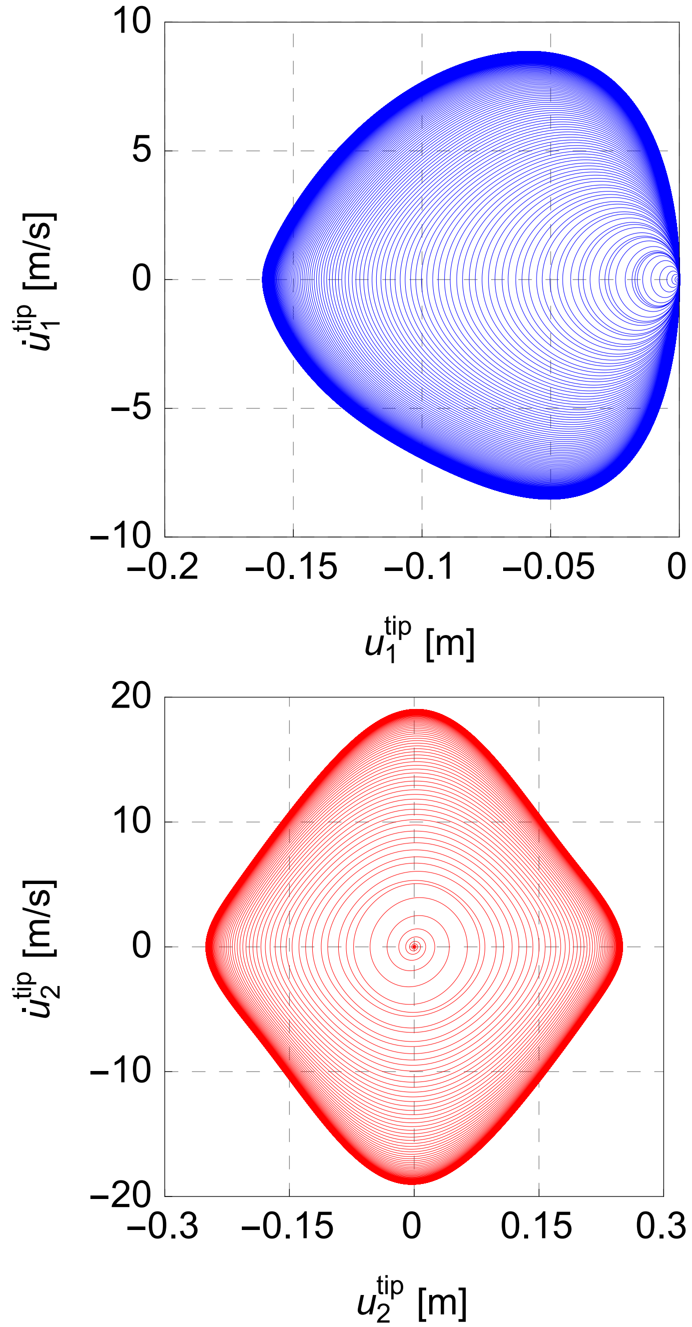

Figure 16. Velocities $\dot{u}_1$ (upper part) and $\dot{u}_2$ (lower part) as functions of the displacements u_1 and u_2, showing the achievement of a limit cycle for the Beck's column (with internal, but not external) dissipation.

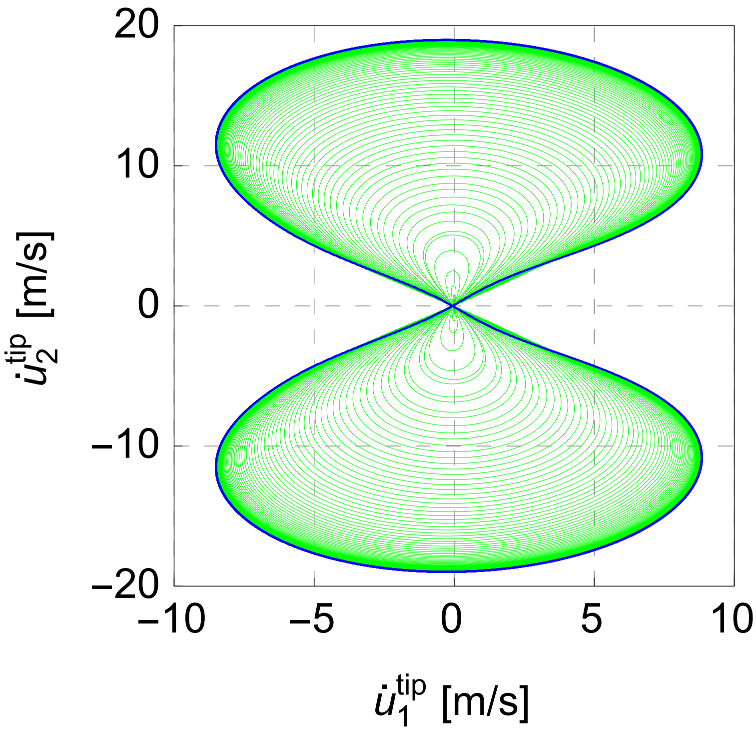

Figure 17. Velocity $\dot{u}_2$ as function of the velocity $\dot{u}_1$, showing the achievement of a limit cycle for the Beck's column (with internal, but not external) dissipation.

2.10 Follower forces from Coulomb friction

The way to generate a follower force from Coulomb friction is shown in Fig. 18, referred to the Ziegler double pendulum. The idea is to mount a little wheel (of negligible rotational inertia) on the end of the pendulum and to force it to slide against a plate with a contact force which can be calibrated. Assuming that the sliding is governed by a simple Coulomb law, the force transmitted at the rod end is: (i.) coaxial to the rod (because the wheel is free of rotating and cannot transmit any orthogonal force) and (ii.) proportional, through a friction coefficient, to the load creating the contact force between the wheel and the plate.

In this way an extremely orthotropic friction is introduced, which transmits only a highly directional force, coaxial to the second rod of the Ziegler

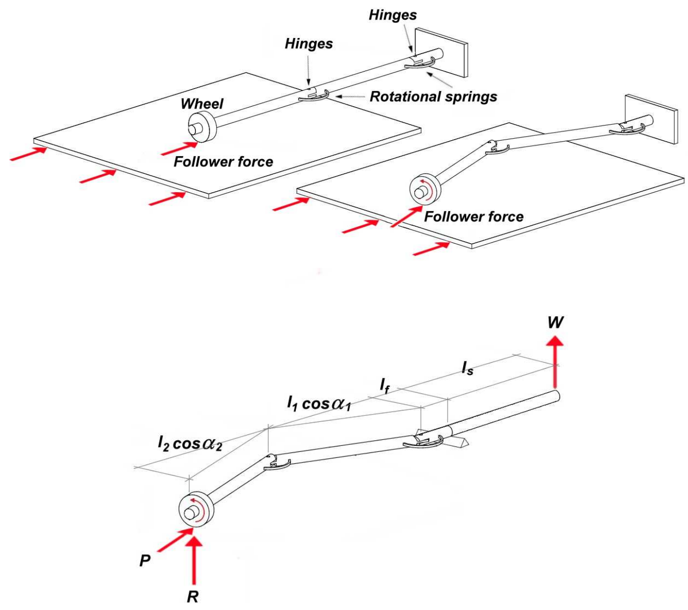

Figure 18. The way to produce a force coaxial to a rod from sliding friction; a freely rotating wheel of negligible mass is mounted at the end of the Ziegler double pendulum and is constrained to slide against a rigid plate (upper part). The way of calibrating the force which compresses the wheel against the plate is to use the Ziegler double pendulum itself as a lever subject to a load W generating a contact force R and thus the follower force P by friction (lower part).

double pendulum.

The scheme to generate a tangentially follower force is an idealization, so that its practical realization can introduce difficulties. However, Bigoni and Noselli (2011) have designed, manufactured and tested a device and have shown that it works in reality, with negligible discrepancies with respect to the conceptual scheme. Without entering into details (the interested reader is referred to Bigoni and Noselli, 2011), it was possible to measure the onset of flutter and divergence instability in terms of applied loads (Fig. 19) and to measure the time variation of the accelerations at the end of the double pendulum (Fig. 20).

Results shown in Fig. 19 demonstrate that a critical load for flutter and divergence instability is found and that the experiments support the

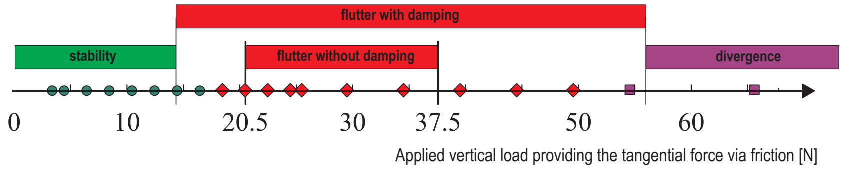

Figure 19. Experimental investigation on flutter and divergence instability with the apparatus sketched in Fig. 18. An increasing vertical load (producing the follower force via friction) is applied for a fixed sliding velocity of the plate against the wheel (50 mm/s). Experimental results are shown with spots and theoretical predictions are reported with horizontal bars. The model in which viscosity is absent 'from the beginning' predicts flutter (divergence) instability to occur at a load higher (smaller) than the load calculated when viscosity is present. In particular, the flutter (divergence) load with viscosity is 0.70 (1.49) times the value calculated in the absence of viscosity. Therefore the experimental results provide evidence of the destabilizing effect of viscosity.

conclusion that viscosity is a destabilizing factor. Fig. 20 shows that the measured acceleration at the end of the structure displays an oscillation initially blowing-up and later converging into a limit cycle.

The scratch left by the sliding wheel on the plate (highlighted with red spots) is visible in a photo reported in Fig. 21, where also the nonlinear solution is indicated (with a white curve). It can be pointed out in general that a definite agreement is observed between all experimental results and the model predictions.

The experimental apparatus designed by Bigoni and Noselli can be developed to test continuously deformable structures. A new device has been recently designed, manufactured, and tested by Bigoni et al. (2018). This device allows for new testings on the Beck's and Pflüger rods, shows that the Beck's model of tangentially follower force can be realized in practice, and provides the first experimental evidence that the viscous dissipation decreases the flutter load.

2.11 Self-oscillating systems

The realization of the Ziegler double pendulum through frictional sliding against an external plate is an example of self-oscillating system[5], in

[5] Self-oscillators are distinct from forced and parametric resonators, in which the power that sustains the motion must be externally modulated.

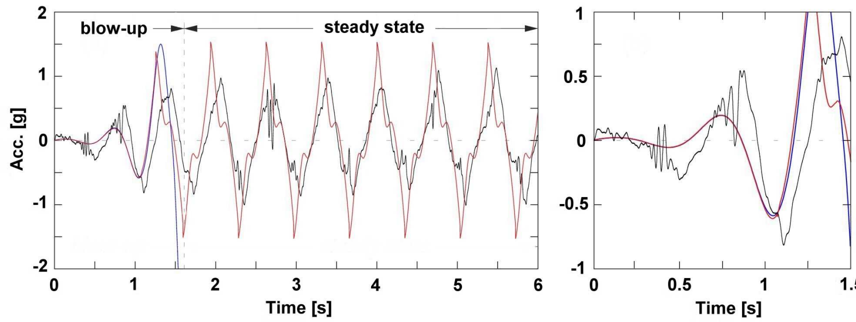

Figure 20. Measured acceleration (at the end of the Ziegler double pendulum) versus time (6 seconds are reported on the left) during a flutter test, performed with the apparatus sketched in Fig. 18 for a load in the middle of the flutter region and a plate velocity of 75 mm/s. The part of the figure on the right is a detail of the part on the left, referred to the initial 1.5 s time interval. Results of a numerical nonlinear (and linear) simulation at the same load and with initial conditions $\alpha_1 = \alpha_2 = 0.5°$ are reported in red (in blue). The solution of the linear equations (blue curve) has been interrupted at 1.5 s since the blow-up was too high. Note the initial increase in the amplitude of the acceleration denoting flutter (well captured even by the linearized viscoelastic analysis), and the following stabilization (well captured by the nonlinear analysis) into a limit cycle.

which a input of steady energy (the frictional force transmitted from the plate to the structure in the present case), lacking periodicity, induces and maintains a self-oscillation of constant frequency (Jenkins, 2013). In other words, the complex 'Ziegler double pendulum-external plate' displays, in the flutter region, self-excited vibrations, in which the oscillating system draws energy from the plate, a mechanism similar to wind induced oscillations of suspension bridges and iced telephone wires.

3 Flutter in frictional solids

Until now the presentation was limited to structures. Now elastoplastic solids will be addressed with the purpose of showing that, when frictional behaviour is taken into account, phenomena akin to flutter and divergence in structural systems may occur even in a continuous medium.

Micromechanisms such as sliding between grains or at micro-fissures are typical of granular or rock-like materials and introduce effects of friction in

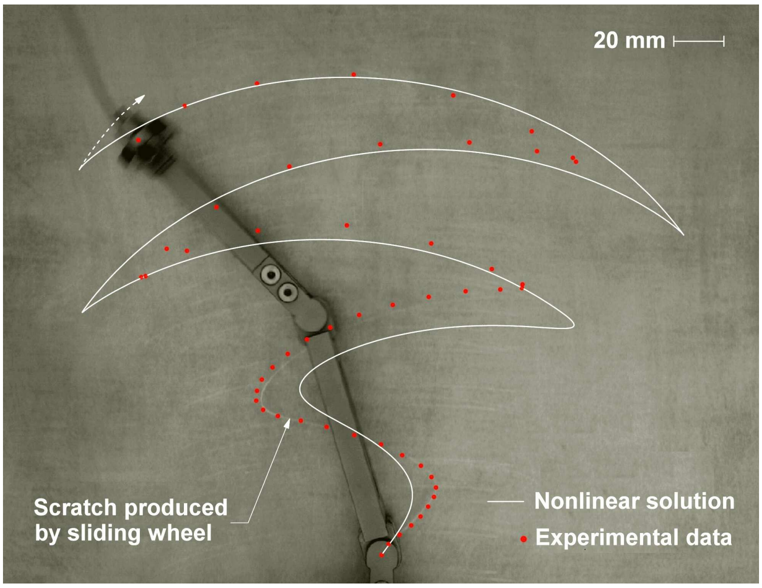

Figure 21. The scratch left by the wheel on the plate of the apparatus shown in Fig. 18, compared with the nonlinear solution (obtained numerically), for a load in the middle of the flutter region and a plate velocity of 100 mm/s. Initial conditions $\alpha_1 = \alpha_2 = 0°$ and $\dot{\alpha}_1 = \dot{\alpha}_2 = 0.5\,\text{rad/s}$ have been used to produce the numerical results. The red spots along the scratches are positions of the wheel corresponding to photos taken with a high speed camera; the scratch left during the experiment is clearly visible in the initial part of the test, not evidencing detachments. The whole sequence corresponds to a 2.04 s interval of time.

the inelastic constitutive modelling of solids. As a consequence, this modelling is characterized by *pressure-sensitivity of yielding* (in other words, an increase with the mean pressure of the shear stress needed to produce yielding) and *dilatant/contractant inelastic deformation*. Consideration of these constitutive features leads to the so-called 'nonassociative elastoplasticity', introduced by Mróz (1963, 1966), Mandel (1962, 1966) and Maier (1970), which can be thought as the counterpart of the model of contact with Coulomb friction in continuum mechanics.

3.1 Contact with Coulomb friction vs. nonassociative elastoplasticity

The close analogy between the equations governing contact between solids with Coulomb friction and the constitutive equations of nonassociative elastoplasticity can be appreciated by the simple model illustrated below with reference to a masonry-like material.

A typical contact between two 'bricks' is sketched on the left in Fig. 22, which is idealized with the simple model reported on the center in the same figure. In particular, a point mass capable of moving only in the horizontal direction is attached to two springs of stiffness k_N and k_T. The vertical displacement u_N of the end of the vertical spring (subject to the compressive force p_N) is purely reversible (and due to the spring deformation only), while the displacement u_T of the end of the horizontal spring (subject to the tangential force p_T) is the sum of the reversible deformation of the spring itself, plus a possible slip u_T^s of the point mass on the rigid horizontal constraint.

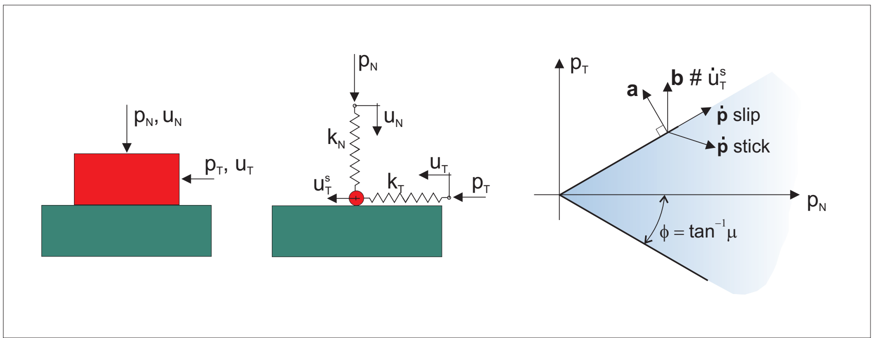

Figure 22. Contact with friction between two 'bricks' (left); a simple model of this, involving Coulomb friction (center); the Coulomb criterion of friction (right). Note the normal **a** to the Coulomb criterion and direction of slip **b** (the symbol '$\sharp$' means 'parallel'). Force 'points' $\{\mathbf{p}\} = \{p_N, p_T\}$ inside the criterion (grey zone) correspond to stick, while for points at the boundary of the criterion stick or slip may occur, depending on the direction of the rate $\dot{\mathbf{p}} = \{\dot{p}_N, \dot{p}_T\}$; in particular, stick (slip) corresponds to $\dot{\mathbf{p}} \cdot \mathbf{a} < 0$ $(= 0)$. Note that the non-parallelism of **a** to **b** implies that the model does not obey the so-called 'normality (or associativity) rule', which is $\mathbf{a}\sharp\mathbf{b}$, so that the model is 'nonassociative'.

The analysis is limited to the condition of *contact* (so that separation and the so-called 'grazing' are not considered, see Radi et al., 1999), corresponding to a compressive (assumed positive) normal force $p_N > 0$.

> *The Coulomb friction condition*, playing the role of the yield condition in plasticity, sets a limit to the possible components p_T, p_N of the force vector $\mathbf{p}$ in the form
>
> $$f(p_N, p_T) \leq 0, \tag{127}$$
>
> where
>
> $$f(p_N, p_T) = |p_T| - \mu p_N, \tag{128}$$
>
> in which μ is the friction coefficient. A geometrical interpretation of criterion (127) is given in Fig. 22 on the right: force states $\mathbf{p}$, represented as points of coordinates p_N, p_T, cannot lie outside the region bounded by the two inclined lines, which graphically represent the Coulomb yield criterion.

Inside the Coulomb criterion: stick When condition (127) is satisfied with the strict inequality '$<$' (corresponding to elastic behaviour in plasticity), *stick* occurs, so that there cannot be slip, $\dot{u}_T^s = 0$, and the corresponding behaviour is reversible and governed by the linear relation

$$\mathbf{p} = \mathbf{E}\mathbf{u}, \qquad \begin{bmatrix} p_N \\ p_T \end{bmatrix} = \begin{bmatrix} k_N & 0 \\ 0 & k_T \end{bmatrix} \begin{bmatrix} u_N \\ u_T \end{bmatrix}, \tag{129}$$

where $\mathbf{E}$ is the matrix collecting the elastic stiffness of the springs.

At the boundary of the Coulomb criterion: stick/slip When condition (127) is satisfied with the equality '$=$', both *slip* ($\dot{u}_T^s \neq 0$) or *stick* ($\dot{u}_T^s = 0$) (corresponding to plastic flow or elastic unloading in plasticity) may occur.

In particular, stick (or slip) occurs if the rate of force is 'directed' inward (or tangential to) the friction condition (Fig. 22), namely

$$\mathbf{a} \cdot \dot{\mathbf{p}} \quad \begin{cases} < 0, & \text{stick}, \\ = 0, & \text{slip}, \end{cases} \tag{130}$$

where $\mathbf{a}$ is the gradient of f

$$[\mathbf{a}] = \left[\frac{\partial f}{\partial \mathbf{p}}\right] = [-\mu, \, \operatorname{sgn} p_T]^T. \tag{131}$$

For stick behaviour, the response is purely reversible, namely

$$|p_T| - \mu p_N = 0, \quad \text{and} \quad \mathbf{a} \cdot \dot{\mathbf{p}} < 0, \quad \Longrightarrow \quad \dot{\mathbf{p}} = \mathbf{E}\dot{\mathbf{u}}, \tag{132}$$

but slip is governed by rate equations.

Rate equations governing the slip For slip behaviour, the rate equations for contact can be obtained from the following three assumptions.

- 1. *Additive decomposition of slip into reversible and irreversible rates* (analogous in plasticity to the decomposition into elastic and plastic rates)

$$\dot{\mathbf{u}} = \dot{\mathbf{u}}^r + \dot{\mathbf{u}}^s, \tag{133}$$

where the superimposed dot denotes derivative with respect to a time-like parameter, governing the loading program.

- 2. *The rate of force is related to the reversible rate of slip* (analogous in plasticity to the rule that the rate of stress is related, through the elastic fourth-order tensor, to the elastic deformation rate)

$$\dot{\mathbf{p}} = \mathbf{E}\dot{\mathbf{u}}^r. \tag{134}$$

- 3. The *slip rule* (analogous in plasticity to the plastic flow rule)

$$\dot{\mathbf{u}}^s = \dot{\lambda}\,\mathbf{b}, \qquad \dot{\lambda} \geq 0, \tag{135}$$

where $\dot{\lambda}$ is a non-negative slip multiplier and $\mathbf{b}$ rules the direction of the rate of slip, so that in the case of Fig. 22

$$[\mathbf{b}] = [0,\, \operatorname{sgn} p_T]^T. \tag{136}$$

Note that $\mathbf{b}$ is not parallel to $\mathbf{a}$, so that in the representation of Fig. 22 (on the right) it is not normal to the Coulomb friction condition. The model is therefore said 'not to follow the normality rule' or to be 'nonassociative', meaning that the so-called 'associativity' or 'normality' rule corresponds to the situation in which $\mathbf{b}$ is parallel to $\mathbf{a}$.

Prager consistency The rate constitutive equations for contact slip can be obtained from the so-called 'consistency equation' [the analogous in plasticity of the Prager (1949) consistency condition], expressing the fact that since the force cannot ever violate the condition of friction, slip may occur only when the rate of force remains tangential to the friction condition, equation $(130)_2$, so that the following condition is obtained

$$\mathbf{a} \cdot \dot{\mathbf{p}} = 0, \quad \Longleftrightarrow \mathbf{a} \cdot \left(\mathbf{E}\dot{\mathbf{u}} - \dot{\lambda}\mathbf{E}\mathbf{b}\right) = 0, \tag{137}$$

from which $\dot{\lambda}$ can be calculated in the form

$$|p_T| - \mu p_N = 0, \quad \text{and} \quad \mathbf{a} \cdot \dot{\mathbf{p}} = 0, \quad \Longrightarrow \quad \dot{\lambda} = \frac{\mathbf{a} \cdot \mathbf{E}\dot{\mathbf{u}}}{\mathbf{a} \cdot \mathbf{E}\mathbf{b}}, \tag{138}$$

so that the slip/stick condition becomes

$$\frac{\mathbf{a} \cdot \mathbf{E}\dot{\mathbf{u}}}{\mathbf{a} \cdot \mathbf{E}\mathbf{b}} \begin{cases} > 0 & \text{slip} \\ \\ < 0 & \text{stick} \end{cases} \tag{139}$$

while the transition condition $\mathbf{a} \cdot \mathbf{E}\dot{\mathbf{u}} = 0$ represents the so-called 'neutral loading'.

Rate equations for slip in final, incrementally-nonlinear form The following rate constitutive equations for contact with friction are finally deduced

$$\dot{\mathbf{p}} = \begin{cases} \mathbf{E}\dot{\mathbf{u}}, & \text{if} \quad |p_T| - \mu p_N < 0, \\ \\ \mathbf{E}\dot{\mathbf{u}} - \dfrac{\langle \mathbf{a} \cdot \mathbf{E}\dot{\mathbf{u}} \rangle}{\mathbf{a} \cdot \mathbf{E}\mathbf{b}} \mathbf{E}\mathbf{b} & \text{if} \quad |p_T| - \mu p_N = 0, \end{cases} \tag{140}$$

which, in the case considered in Fig. 22, become *the rate equations of contact with Coulomb friction*

$$\dot{p}_N = k_N \dot{u}_N, \qquad \dot{p}_T = k_T \dot{u}_T - \langle -\mu\, k_N \dot{u}_N + k_T \dot{u}_T \operatorname{sgn} p_T \rangle \operatorname{sgn} p_T. \tag{141}$$

The operator $\langle \cdot \rangle$ in equations (140) and (141) is the so-called 'Macaulay bracket', defined for every $\alpha \in \mathbb{R}$ as $\langle \alpha \rangle = (|\alpha| + \alpha)/2$.

> The Macaulay bracket operator provides *the rate piecewise linearity (a simple form of incremental nonlinearity, which distinguishes between slip and stick) typical of elastoplasticity (where 'stick' is replaced by 'elastic unloading' and 'slip' by 'plastic loading').*

Equations (140) are formally identical to the rate constitutive equations of nonassociative ideal (i.e. with null hardening) elastoplasticity. In the equations of elastoplasticity $\dot{\mathbf{p}}$ is replaced by the rate of stress, $\dot{\mathbf{u}}$ by the deformation rate, $\mathbf{a}$ by the yield function gradient, $\mathbf{b}$ by the plastic flow mode tensor and $\mathbf{E}$ by the fourth-order elastic tensor. In the problem of contact with friction, exactly as for the rate constitutive equations of nonassociative elastoplasticity, it turns out that:

- The contact condition (140) is written *in a rate form and cannot be resolved into equations involving finite quantities* (to understand this important point it suffices to consider that the knowledge of a finite displacement u_T at given value of vertical force p_N does not determine the tangential force p_T, since the irreversible part of displacement u_T^s is not known and this can be obtained only through integration in time of the rate equations).

- The rate equations are incrementally nonlinear and characterized by an elastic

$$\dot{\mathbf{p}} = \mathbf{E}\dot{\mathbf{u}}, \tag{142}$$

and a plastic

$$\dot{\mathbf{p}} = \mathbf{C}\dot{\mathbf{u}}, \qquad \mathbf{C} = \mathbf{E} - \frac{1}{\mathbf{a} \cdot \mathbf{E}\mathbf{b}} \mathbf{E}\mathbf{b} \otimes \mathbf{E}\mathbf{a}, \tag{143}$$

branch [the symbol '$\otimes$' is the dyadic product].

- *The constitutive tensor* $\mathbf{C}$ *characterizing the plastic branch is not symmetric*; therefore the structure of problems involving friction is not self-adjoint. Note that the fact that $\mathbf{C}$ is not symmetric follows from the difference between $\mathbf{a}$ and $\mathbf{b}$. The former vector is *normal* to the friction criterion (see Fig. 22), while the latter is not. Therefore, the model lacks 'normality' or in other words is 'nonassociative', in the sense that the slip rule 'associated' to the friction criterion requires $\mathbf{b}$ to be parallel to $\mathbf{a}$.

3.2 The rate equations of nonassociative elastoplasticity for frictional solids

Elastoplasticity is based on the concept of yield function

$$f(\boldsymbol{\sigma}, \mathcal{K}) \leq 0, \tag{144}$$

depending on the stress $\boldsymbol{\sigma}$ and on a set of internal variables $\mathcal{K}$ governing the inelastic deformation of the material. Negative values of f determine elastic states, for which only elastic deformation is possible, while plastic flow may occur only when $f = 0$. Positive values of f are excluded.

The rate equations of incremental elastoplasticity can be derived from the following four assumptions:

- 1. *Additive decomposition of elastic,* $\dot{\boldsymbol{\epsilon}}^e$*, and plastic,* $\dot{\boldsymbol{\epsilon}}^p$*, strain rates*

$$\dot{\boldsymbol{\epsilon}} = \dot{\boldsymbol{\epsilon}}^e + \dot{\boldsymbol{\epsilon}}^p, \tag{145}$$

where $\dot{\boldsymbol{\epsilon}}$ is the rate of strain, so that the superimposed dot denotes derivative with respect to a time-like parameter, governing the loading program.

- 2. *The rate of stress* $\dot{\boldsymbol{\sigma}}$ *is related to the rate of elastic strain*
$$\dot{\boldsymbol{\sigma}} = \mathcal{E}[\dot{\boldsymbol{\epsilon}}^e], \tag{146}$$
through a fourth-order elastic tensor $\mathcal{E}$.
- 3. The *plastic flow rule*
$$\dot{\boldsymbol{\epsilon}}^p = \dot{\lambda}\,\mathbf{P}, \qquad \dot{\lambda} \geq 0, \tag{147}$$
where $\dot{\lambda}$ is a non-negative plastic multiplier and $\mathbf{P}$ is a symmetric, second-order tensor, which rules the direction of the rate of plastic strain.
- 4. The *hardening rule*
$$-\frac{\partial f}{\partial \mathcal{K}} \cdot \dot{\mathcal{K}} = \dot{\lambda} H, \tag{148}$$
where H is the hardening modulus, positive for hardening, null for ideal plasticity, and negative for softening.

Imposing the Prager consistency, namely, $\dot{f} = 0$ for plastic flow, yields
$$\dot{f} = \frac{\partial f}{\partial \boldsymbol{\sigma}} \cdot \dot{\boldsymbol{\sigma}} + \frac{\partial f}{\partial \mathcal{K}} \cdot \dot{\mathcal{K}} = \mathbf{Q} \cdot \mathcal{E}[\dot{\boldsymbol{\epsilon}}] - \dot{\lambda}\mathbf{Q} \cdot \mathcal{E}[\mathbf{P}] - \dot{\lambda} H = 0, \tag{149}$$
from which the plastic multiplier is obtained
$$\dot{\lambda} = \frac{< \mathbf{Q} \cdot \mathcal{E}[\dot{\boldsymbol{\epsilon}}] >}{H + \mathbf{Q} \cdot \mathcal{E}[\mathbf{P}]}, \tag{150}$$
where $<>$ denotes the Macaulay brackets.

As a conclusion, the rate equations of elastoplasticity can be written as
$$\dot{\boldsymbol{\sigma}} = \begin{cases} \mathcal{E}[\dot{\boldsymbol{\epsilon}}], & \text{if } f < 0, \\[2ex] \mathcal{E}[\dot{\boldsymbol{\epsilon}}] - \dfrac{< \mathbf{Q} \cdot \mathcal{E}[\dot{\boldsymbol{\epsilon}}] >}{g} \mathcal{E}[\mathbf{P}], & \text{if } f = 0, \end{cases} \tag{151}$$
where the plastic modulus g (assumed strictly positive) is defined as
$$g = H + \mathbf{Q} \cdot \mathcal{E}[\mathbf{P}]. \tag{152}$$

The elastic branch of the constitutive equations (151) is simply the elastic fourth-order tensor, $\mathcal{E}$, while the plastic branch can be written in a form similar to (143), namely
$$\mathcal{C} = \mathcal{E} - \frac{1}{g}\mathcal{E}[\mathbf{P}] \otimes \mathcal{E}^T[\mathbf{Q}], \tag{153}$$
which shows the following interesting features:

- Assuming the major symmetry of $\mathcal{E}$, the operator $\mathcal{C}$ is symmetric if and only if $\mathbf{P}$ is proportional to $\mathbf{Q}$, in other words when (for a scalar α) $\mathbf{P} = \alpha\mathbf{Q}$;
- Defining the stiffness of $\mathcal{C}$ in terms of the second-order work $\dot{\boldsymbol{\epsilon}} \cdot \mathcal{C}[\dot{\boldsymbol{\epsilon}}]$, it is evident that the elastic stiffness can be smaller than the elastoplastic stiffness, when $(\dot{\boldsymbol{\epsilon}} \cdot \mathcal{E}[\mathbf{P}]) \left(\mathbf{Q}\mathcal{E}^T[\dot{\boldsymbol{\epsilon}}]\right) < 0$.

The normality rule corresponds to $\mathbf{P} = \mathbf{Q}$, which determines the associative elastoplastic model, and corresponds to a symmetric operator (153). Generally speaking, the choice of $\mathbf{P}$ as related to $\mathbf{Q}$ should be based on experimental results. These show that many solids (and in particular granular materials) exhibit a peculiar kind of non-associativity, involving only the volumetric part of plastic deformation. This case of special interest corresponds to so-called *deviatoric associativity*, where the deviatoric parts of $\mathbf{P}$ and $\mathbf{Q}$ are aligned, so that

$$\mathbf{P} = \chi_1 \hat{\mathbf{S}} + \frac{\chi_2}{3}\mathbf{I}, \qquad \mathbf{Q} = \psi_1 \hat{\mathbf{S}} + \frac{\psi_2}{3}\mathbf{I}, \tag{154}$$

where $\hat{\mathbf{S}} \in \mathrm{Sym}$ is traceless, χ_1 and ψ_1 are assumed strictly positive. The parameters ψ_2 and χ_2 respectively describe the *pressure-sensitivity* and the *dilatancy* (when $\chi_2 > 0$) or *contractility* (when $\chi_2 < 0$) of the material. In the case of the Drucker-Prager model and the flow rule nonassociativity used, among many others, by Bigoni and Loret (1999), the parameters can be rewritten as

$$\begin{aligned} &\chi_1 = \cos\chi, \quad \chi_2 = \sqrt{3}\sin\chi, \psi_1 = \cos\phi, \quad \psi_2 = \sqrt{3}\sin\phi, \\ &\hat{\mathbf{S}} = \frac{\mathrm{dev}\boldsymbol{\sigma}}{|\mathrm{dev}\boldsymbol{\sigma}|}, \end{aligned} \tag{155}$$

where $\mathrm{dev}\boldsymbol{\sigma} = \boldsymbol{\sigma} - \mathbf{I}\,(\mathrm{tr}\boldsymbol{\sigma}/3)$ is the deviatoric stress.

3.3 The propagation of incremental plane waves

The rate equations of elastoplasticity are incrementally nonlinear, in the sense that the rate response is different for plastic loading or elastic unloading, a property evidenced by presence of the Macaulay brackets in equation (151). Therefore, every solution, even in rate form, is the solution of a nonlinear problem. Under this nonlinearity assumption, the usually simple problem of sinusoidal wave propagation in an infinite body becomes complicated (Bigoni and Petryk, 2002). Therefore, wave propagation in plasticity is usually analyzed for acceleration waves, viewed as propagating discontinuity surfaces for the acceleration (Hill, 1962; Mandel, 1962; Raniecki, 1976; Bigoni, 2012). However, the acceleration wave approach for plastic waves provides exactly the same result that it is found for sinusoidal incremental waves restricted to the loading branch of the constitutive operator. Therefore, to simplify the treatment, incremental disturbances in the form of plane sinusoidal waves will be considered in the following with reference to the plastic branch of the constitutive equation (151), so that 'rates' will be identified with 'increments', namely, $\dot{\boldsymbol{\sigma}}$ becomes the increment of stress $\Delta\boldsymbol{\sigma}$ and $\dot{\boldsymbol{\epsilon}}$ becomes the gradient of an incremental displacement, $\nabla\mathbf{w}$.

An infinite, homogeneously deformed and stressed elastoplastic material is considered, so that equilibrium and compatibility are trivially satisfied. Any incremental dynamic solution must satisfy the incremental equations of motion (when body forces are absent)

$$\mathrm{div}\Delta\boldsymbol{\sigma} = \rho\ddot{\mathbf{w}}, \tag{156}$$

where ρ is the mass density of the material and $\ddot{\mathbf{w}}$ is an incremental acceleration. Incremental solutions are sought in the following sinusoidal wave form

$$\mathbf{w} = \mathrm{Re}\left\{\mathbf{a}e^{ik(\mathbf{n}\cdot\mathbf{x}\pm ct)}\right\}, \tag{157}$$

where $i = \sqrt{-1}$, $\mathbf{n}$ is the unit vector of propagation, $\mathbf{a}$ is the (possibly complex) wave amplitude vector, k is the (positive) wave number, c is the (possibly complex) wave speed.

Adopting the complex notation, the gradient and the time derivative of equation (157) are

$$\nabla\mathbf{w} = ik\,\mathbf{w}\otimes\mathbf{n}, \quad \dot{\mathbf{w}} = \pm ick\,\mathbf{w}, \tag{158}$$

while the second gradient and second time-derivative are

$$\nabla\left(\nabla\mathbf{w}\right) = -k^2\,\mathbf{w}\otimes\mathbf{n}\otimes\mathbf{n}, \quad \ddot{\mathbf{w}} = -c^2k^2\,\mathbf{w}. \tag{159}$$

Inserting equations (159) into the momentum balance (156) leads to the propagation condition

$$(\mathbf{A}(\mathbf{n}) - c^2\mathbf{I})\mathbf{a} = \mathbf{0}, \tag{160}$$

where $\mathbf{A}(\mathbf{n})$ is the acoustic tensor defined, for every vector $\mathbf{g}$, as

$$\mathbf{A}(\mathbf{n})\mathbf{g} = \frac{1}{\rho}\mathcal{E}[\mathbf{g}\otimes\mathbf{n}]\mathbf{n} - \frac{\mathbf{g}\cdot\mathcal{E}^T[\mathbf{Q}]\mathbf{n}}{\rho g}\mathcal{E}[\mathbf{P}]\mathbf{n}, \tag{161}$$

so that the squared propagation velocities c^2 are the eigenvalues of the acoustic tensor corresponding to the loading branch of the constitutive elastoplastic operator.

On the basis of the nature of the three eigenvalues of the acoustic tensor, the following nomenclature can be introduced (Rice, 1977).

In CISM Lecture Notes No. 586 "Dynamic Stability and Bifurcation in Nonconservative Mechanics" (Ch. 1), edited by: D. Bigoni and O. Kirillov, Springer, ISBN 978-3-319-93721-2, doi 10.1007/978-3-319-93722-9

- *Stability* occurs when all values for c^2 are strictly positive, so that waves propagate sinusoidally with a finite speed;
- *divergence instability* corresponds to a real and negative value for c^2, so that waves grow exponentially during propagation;
- *flutter instability* corresponds to two complex conjugate eigenvalues c^2, so that an oscillation blowing-up in time is predicted.

The following conclusions can be drawn.

- In the case when $\mathcal{E}$ is hyperelastic (and thus possesses all symmetries) and for the associative flow rule $\mathbf{P} = \mathbf{Q}$, the eigenvalues c^2 are always real and the corresponding eigenspaces orthogonal, so that flutter instability is excluded.
- Therefore, a necessary condition for flutter instability is that the plastic flow be nonassociative, $\mathbf{P} \neq \mathbf{Q}$.

It may also be easily seen from the form of the acoustic tensor (161) that the nonassociativity of the flow rule opens the possibility that a wave involving plastic loading can travel faster than an elastic unloading wave, characterized by the acoustic tensor $\mathbf{A}_{el}(\mathbf{n})$ defined, with reference to an arbitrary vector $\mathbf{g}$, as

$$\mathbf{A}_{el}(\mathbf{n})\mathbf{g} = \frac{1}{\rho}\mathcal{E}[\mathbf{g} \otimes \mathbf{n}]\mathbf{n}. \tag{162}$$

This possibility, called 'achronic state', occurs when a plastic eigenvalue is larger than any of the elastic eigenvalues and leads to possible dynamical instabilities (Sandler and Rubin, 1987; Pucik et al., 2015; Burghardt and Brannon, 2015; Brannon, 2007).

3.4 Strain localization into planar bands

Considering an infinite solid body, subject to a continued path of uniform strain, the condition that an incremental (or rate) strain localizes into a planar band of infinite extent can be analyzed in terms of vanishing speed of a planar plastic wave, $c = 0$, which corresponds to the singularity of the acoustic tensor $\mathbf{A}(\mathbf{n})$, equation (161), for at least one direction $\mathbf{n}$, namely

$$\det \mathbf{A}(\mathbf{n}) = 0, \qquad \text{strain localization condition.} \tag{163}$$

Assuming that the elastic fourth-order tensor $\mathcal{E}$ be positive definite and assuming $\rho = 1$, the condition (163) can be rewritten as

$$\det\left[\mathbf{I} - \frac{1}{g}\mathbf{A}_{el}^{-1}(\mathbf{n})\mathbf{p} \otimes \mathbf{q}\right] = 0, \tag{164}$$

where

$$\mathbf{p} = \mathcal{E}[\mathbf{P}]\mathbf{n}, \quad \mathbf{q} = \mathcal{E}^T[\mathbf{Q}]\mathbf{n}. \tag{165}$$

Using the algebraic property $\det(\mathbf{I} + \mathbf{a} \otimes \mathbf{b}) = 1 + \mathbf{a} \cdot \mathbf{b}$, the strain localization condition (164) can be written in terms of a critical value of the plastic modulus

$$g_{cr}^E = \mathbf{q} \cdot \mathbf{A}_{el}^{-1}(\mathbf{n})\mathbf{p}. \tag{166}$$

The fact that condition (163), and therefore (166), corresponds to the possibility of a localization of strain can be understood by considering that the emergence of a discontinuity surface (of unit normal vector $\mathbf{n}$) for the strain rate during a continued homogeneous deformation is conditioned by the fulfillment of the following two conditions.

- Incremental equilibrium across the discontinuity surface, which requires continuity of the traction rate

$$[[\dot{\boldsymbol{\sigma}}]]\mathbf{n} = 0, \tag{167}$$

  where the bracket $[[\cdot]]$ denotes the jump across the surface of the relevant argument.
- Validity of the Maxwell compatibility conditions, which specify a form for the jump in the gradient of the velocity $\nabla\dot{\mathbf{u}}$ across the discontinuity surface

$$[[\nabla\dot{\mathbf{u}}]] = \mathbf{g} \otimes \mathbf{n}, \tag{168}$$

  where $\mathbf{g}$ represents the jump in the normal derivative of the gradient of velocity.

The condition (167) has a simple mechanical interpretation, while the condition (168) is more complicated and merits a detailed explanation. A field quantity which is prescribed to remain continuous across a surface, but may admit a discontinuity in its gradient, has to remain continuous when the directional derivatives are taken tangential to the discontinuity surface. Consideration of the tangential derivative leads to equation (168). This point can be exemplified with the following two examples.

Example 1. Twinning shear deformation A deformation such as that sketched in Fig. 23 is often found in crystals and is composed of two mirror-like simple shears, where the symmetry line defines the 'twinning plane'.

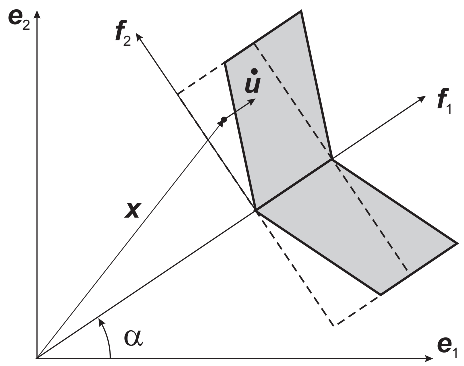

Figure 23. Twinning shear deformation of plane $\mathbf{f}_1$, across which the incremental displacement $\dot{\mathbf{u}}$ is continuous, but not its gradient.

An incremental displacement $\dot{\mathbf{u}}$ such as that reported in Fig. 23 has the following form

$$\dot{\mathbf{u}} = |\mathbf{x} \cdot \mathbf{f}_2| \mathbf{f}_1, \tag{169}$$

where $\mathbf{f}_1$ is the unit vector defining the twinning line and $\mathbf{f}_2$ is its orthogonal complement to define a basis. The gradient of the incremental displacement is

$$\nabla \dot{\mathbf{u}} = \text{sgn}(\mathbf{x} \cdot \mathbf{f}_2) \mathbf{f}_1 \otimes \mathbf{f}_2, \tag{170}$$

where $\text{sgn}(\mathbf{x} \cdot \mathbf{f}_2)$ provides the jump in the derivative orthogonal to the twinning plane. Therefore, the jump in the gradient of incremental displacement is

$$[[\nabla \dot{\mathbf{u}}]] = 2\mathbf{f}_1 \otimes \mathbf{f}_2, \tag{171}$$

which is in the fom (168), because $\mathbf{f}_2$ is the normal to the discontinuity plane and $2\mathbf{f}_1$ is the jump of the normal derivative of the incremental displacement across the same plane.

Note that in the reference system $\mathbf{e}_1$–$\mathbf{e}_2$

$$\mathbf{f}_1 = \cos\alpha \mathbf{e}_1 + \sin\alpha \mathbf{e}_2, \quad \mathbf{f}_2 = -\sin\alpha \mathbf{e}_1 + \cos\alpha \mathbf{e}_2, \tag{172}$$

condition (170) becomes

$$\begin{aligned} [[\nabla \dot{\mathbf{u}}]] = \quad & 2\left(-\mathbf{e}_1 \otimes \mathbf{e}_1 \sin\alpha\cos\alpha + \mathbf{e}_1 \otimes \mathbf{e}_2 \cos^2\alpha \right. \\ & \left. -\mathbf{e}_2 \otimes \mathbf{e}_1 \sin^2\alpha + \mathbf{e}_2 \otimes \mathbf{e}_2 \sin\alpha\cos\alpha\right), \end{aligned} \tag{173}$$

an expression which 'hiddens' the dyadic structure of the Maxwell compatibility (168).

In CISM Lecture Notes No. 586 "Dynamic Stability and Bifurcation in Nonconservative Mechanics" (Ch. 1), edited by: D. Bigoni and O. Kirillov, Springer, ISBN 978-3-319-93721-2, doi 10.1007/978-3-319-93722-9

Example 2. An incremental deformation is considered where the incremental displacement depends on the variable x_2 only through its absolute value, $y = |x_2|$, so that $\dot{\mathbf{u}} = \dot{\mathbf{u}}(x_1, y, x_3)$ and its gradient in components is

$$\nabla\dot{\mathbf{u}} = \begin{bmatrix} \dot{u}_{1,1} & \text{sgn}(x_2)\dot{u}_{1,y} & \dot{u}_{1,3} \\ \dot{u}_{2,1} & \text{sgn}(x_2)\dot{u}_{2,y} & \dot{u}_{2,3} \\ \dot{u}_{3,1} & \text{sgn}(x_2)\dot{u}_{3,y} & \dot{u}_{3,3} \end{bmatrix}. \tag{174}$$

The jump in the gradient across the plane $x_2 = 0$ of unit normal $\mathbf{e}_2$ can be written as

$$[[\nabla\dot{\mathbf{u}}]] = \begin{bmatrix} 0 & 2\dot{u}_{1,y} & 0 \\ 0 & 2\dot{u}_{2,y} & 0 \\ 0 & 2\dot{u}_{3,y} & 0 \end{bmatrix}, \tag{175}$$

so that the mathematical structure (168) is recovered, namely,

$$[[\nabla\dot{\mathbf{u}}]] = \mathbf{g} \otimes \mathbf{e}_2, \tag{176}$$

with

$$\mathbf{g} = 2\dot{u}_{1,y}\mathbf{e}_1 + 2\dot{u}_{2,y}\mathbf{e}_2 + 2\dot{u}_{3,y}\mathbf{e}_3. \tag{177}$$

The condition for strain localization (163) can now be derived by combining equations (167) and (168) with the plastic branch of the rate constitutive equations (153). Therefore, the mechanical meaning of the condition (163), implying the possibility of a localization of deformation into a planar band, becomes clear.

It should be noted that in the 'standard' case of the associative flow rule, $\mathbf{P} = \mathbf{Q}$, the acoustic tensor is symmetric. Therefore, the usual situation is that, during a uniform strain path of a material, the hardening modulus evolves from a positive value, vanishes for perfectly plastic behaviour, and finally becomes negative for strain softening. During this evolution, the eigenvalues of the acoustic tensor are initially positive and decreasing functions of the strain hardening, so that when a critical value of the hardening modulus is met, one of these eigenvalues vanishes and the plastic deformation starts to localize into a planar band.

After plastic localization occurs, usually (the situation can be much more complicated, see Gajo et al., 2004) the material outside the band starts to

In CISM Lecture Notes No. 586 "Dynamic Stability and Bifurcation in Nonconservative Mechanics" (Ch. 1), edited by: D. Bigoni and O. Kirillov, Springer, ISBN 978-3-319-93721-2, doi 10.1007/978-3-319-93722-9

elastically unload, while the material inside the band continues to deform plastically.

For associative elastoplasticity at small deformation, the critical hardening modulus for strain localization is never positive, so that localization occurs for perfectly plastic or softening behaviour. However, the situation is different both when large deformation effects are taken into account or when the flow rule is nonassociative, in which cases strain localization may occur even during hardening.

3.5 The analysis of the acoustic tensor and flutter instability

The most important results on flutter instability relative to small strain nonassociative elastoplasticity, based on isotropic elasticity, are due to Loret (1992) and Loret et al. (1990) and are now presented following Bigoni (2012) and Bigoni and Zaccaria (1994). Results relative to nonassociative plasticity with anisotropic elastic behaviour were provided by Bigoni and Loret (1999) and Bigoni et al. (2000).

An isotropic elastic tensor $\mathcal{E}$ is assumed in the following for a material with unit mass density, $\rho = 1$, so that the elastic acoustic tensor is

$$\mathbf{A}_{el}(\mathbf{n}) = (\lambda + \mu)\mathbf{n} \otimes \mathbf{n} + \mu \mathbf{I}, \tag{178}$$

where λ and μ are the Lamé constants. The acoustic tensor corresponding to the plastic branch of the constitutive equation (151) is given by

$$\mathbf{A}(\mathbf{n}) = (\lambda + \mu)\mathbf{n} \otimes \mathbf{n} + \mu \mathbf{I} - \frac{1}{g}\mathbf{p} \otimes \mathbf{q}, \tag{179}$$

where

$$\mathbf{q} = \lambda(\mathrm{tr}\mathbf{Q})\mathbf{n} + 2\mu\mathbf{Q}\mathbf{n}, \quad \mathbf{p} = \lambda(\mathrm{tr}\mathbf{P})\mathbf{n} + 2\mu\mathbf{P}\mathbf{n}, \tag{180}$$

are linear functions of $\mathbf{n}$. Assuming that $\mathbf{n} \times \mathbf{q} \neq \mathbf{0}$, the following non-orthogonal dual bases for the three-dimensional Euclidean space are employed

$$\begin{array}{lll} \mathbf{e}_1 = \mathbf{n}, & \mathbf{e}_2 = \mathbf{q}, & \mathbf{e}_3 = \dfrac{\mathbf{n} \times \mathbf{q}}{|\mathbf{n} \times \mathbf{q}|}, \\[2ex] \mathbf{e}^1 = \dfrac{(\mathbf{q}^2)\mathbf{n} - (\mathbf{q} \cdot \mathbf{n})\mathbf{q}}{\mathbf{q}^2 - (\mathbf{q} \cdot \mathbf{n})^2}, & \mathbf{e}^2 = \dfrac{\mathbf{q} - (\mathbf{q} \cdot \mathbf{n})\mathbf{n}}{\mathbf{q}^2 - (\mathbf{q} \cdot \mathbf{n})^2}, & \mathbf{e}^3 = \mathbf{e}_3, \end{array} \tag{181}$$

which satisfy the property $\mathbf{e}^i \cdot \mathbf{e}_j = \delta^i_j$, where δ^i_j is the Kronecker delta.

Projected onto the bases (181), the acoustic tensor writes as

$$[\mathbf{A}] = \begin{bmatrix} \mathbf{e}_1 \cdot \mathbf{A}\mathbf{e}^1 & \mathbf{e}_1 \cdot \mathbf{A}\mathbf{e}^2 & \mathbf{e}_1 \cdot \mathbf{A}\mathbf{e}^3 \\ \mathbf{e}_2 \cdot \mathbf{A}\mathbf{e}^1 & \mathbf{e}_2 \cdot \mathbf{A}\mathbf{e}^2 & \mathbf{e}_2 \cdot \mathbf{A}\mathbf{e}^3 \\ \mathbf{e}_3 \cdot \mathbf{A}\mathbf{e}^1 & \mathbf{e}_3 \cdot \mathbf{A}\mathbf{e}^2 & \mathbf{e}_3 \cdot \mathbf{A}\mathbf{e}^3 \end{bmatrix}, \tag{182}$$

so that the eigenvalue problem for (179) yields the characteristic equation

$$\det \begin{pmatrix} \lambda + 2\mu - \eta & -\frac{1}{g}\mathbf{p} \cdot \mathbf{n} & 0 \\ (\lambda + \mu)\mathbf{q} \cdot \mathbf{n} & \mu - \frac{1}{g}\mathbf{p} \cdot \mathbf{q} - \eta & 0 \\ 0 & -\frac{1}{g}\mathbf{p} \cdot \mathbf{e}_3 & \mu - \eta \end{pmatrix} = 0, \tag{183}$$

where η is the generic eigenvalue of the acoustic tensor (179). The three solutions to the characteristic equation (183) are the eigenvalue μ and the two roots of the polynomial equation:

$$\begin{aligned} \eta^2 - \left(\lambda + 3\mu - \frac{1}{g}\mathbf{p} \cdot \mathbf{q}\right)\eta \quad &+ (\lambda + 2\mu)\left(\mu - \frac{1}{g}\mathbf{p} \cdot \mathbf{q}\right) \\ &+ \frac{1}{g}(\lambda + \mu)(\mathbf{p} \cdot \mathbf{n})(\mathbf{q} \cdot \mathbf{n}) = 0. \end{aligned} \tag{184}$$

Strain localization into a planar band of unit normal $\mathbf{n}$, equation (166), occurs when $\eta = 0$ in equation (184), which corresponds to the following critical condition for the plastic modulus

$$g_{cr}^E(\mathbf{n}) = -\frac{\lambda + \mu}{\mu(\lambda + 2\mu)}(\mathbf{p} \cdot \mathbf{n})(\mathbf{q} \cdot \mathbf{n}) + \frac{\mathbf{p} \cdot \mathbf{q}}{\mu}. \tag{185}$$

Flutter instability is equivalent to the condition that the discriminant Δ of the second-order polynomial in equation (184) assumes negative values. The discriminant can be written as

$$\Delta = \left(\lambda + 3\mu - \frac{1}{g}\mathbf{p} \cdot \mathbf{q}\right)^2 - 4\mu(\lambda + 2\mu)\left(1 - \frac{g_{cr}^E(\mathbf{n})}{g}\right), \tag{186}$$

where $g_{cr}^E(\mathbf{n})$ represents the critical plastic modulus for strain localization at fixed $\mathbf{n}$, equation (185). Therefore, it can be concluded that (Bigoni and Zaccaria, 1994):

> *For a given direction* $\mathbf{n}$*, flutter is always excluded for values of the plastic modulus less than or equal to the critical plastic modulus for strain localization in a band orthogonal to that direction* $\mathbf{n}$.

Straightforward manipulation of the discriminant (186) yields the necessary and sufficient conditions for flutter

$$\boxed{(\mathbf{n}\cdot\mathbf{p})(\mathbf{n}\cdot\mathbf{q}) > 0, \quad \& \quad (\mathbf{n}\cdot\mathbf{p})(\mathbf{n}\cdot\mathbf{q}) - \mathbf{p}\cdot\mathbf{q} > 0, \quad \& \quad g \in (g_1, g_2),} \tag{187}$$

where

$$\boxed{\left.\begin{array}{c} g_1 \\ g_2 \end{array}\right\} = \frac{1}{\lambda+\mu}\left(\sqrt{(\mathbf{n}\cdot\mathbf{p})(\mathbf{n}\cdot\mathbf{q})} \pm \sqrt{(\mathbf{n}\cdot\mathbf{p})(\mathbf{n}\cdot\mathbf{p}) - \mathbf{p}\cdot\mathbf{q}}\right)^2.} \tag{188}$$

If deviatoric associativity (154) is assumed, a simple calculation shows that condition $(187)_2$ is never satisfied, which leads to the conclusion (Loret et al., 1990; Brannon and Drugan, 1993):

> *For elastic-plastic solids in the presence of isotropic elasticity and deviatoric associativity (154) with parameters χ_1 and ψ_1 being strictly positive, complex eigenvalues of the acoustic tensor are excluded.*

However, *coincident eigenvalues are possible.* These may be determined by requiring that the discriminant (186) be null, which occurs when one of the following two conditions is satisfied

$$(\mathbf{n}\cdot\mathbf{p})(\mathbf{n}\cdot\mathbf{q}) = 0, \quad \text{and} \quad g = g_{cr}^C(\mathbf{n}) = -\frac{\mathbf{p}\cdot\mathbf{q}}{\lambda+\mu}, \tag{189}$$

or

$$(\mathbf{n}\cdot\mathbf{p})(\mathbf{n}\cdot\mathbf{q}) = \mathbf{p}\cdot\mathbf{q}, \quad \text{and} \quad g = g_{cr}^C(\mathbf{n}) = \frac{\mathbf{p}\cdot\mathbf{q}}{\lambda+\mu}. \tag{190}$$

Assuming isotropic elasticity and deviatoric associativity (154), it is easy to obtain that

$$\mathbf{p}\cdot\mathbf{q} - (\mathbf{n}\cdot\mathbf{p})(\mathbf{n}\cdot\mathbf{q}) = 4\mu^2\chi_1\psi_1\left(\hat{\mathbf{S}}\mathbf{n}\cdot\hat{\mathbf{S}}\mathbf{n} - (\mathbf{n}\cdot\hat{\mathbf{S}}\mathbf{n})^2\right) \geq 0. \tag{191}$$

Therefore

$$(\mathbf{n}\cdot\mathbf{p})(\mathbf{n}\cdot\mathbf{q}) = 0 \implies \mathbf{p}\cdot\mathbf{q} \geq 0 \implies g_{cr}^C(\mathbf{n}) \leq 0, \tag{192}$$

so that Case (189) is not interesting. Examining Case (190), equation (184) provides two coincident solutions equal to μ. Therefore:

> *The acoustic tensor (for certain $\mathbf{n}$) has an eigenvalue equal to μ, with multiplicity 3, when condition (190) is satisfied.*

Now the critical plastic modulus for such a coalescence can be determined, noting that the following condition holds true at coalescence

$$\hat{\mathbf{S}}\mathbf{n}\cdot\hat{\mathbf{S}}\mathbf{n} = (\mathbf{n}\cdot\hat{\mathbf{S}}\mathbf{n})^2, \tag{193}$$

D. Bigoni and O. Kirillov, Springer, ISBN 978-3-319-93721-2, doi 10.1007/978-3-319-93722-9

and is verified if and only if $\mathbf{n}$ is an eigenvector of $\hat{\mathbf{S}}$, but in this case $\mathbf{n}$ is also an eigenvector of $\mathcal{E}[\mathbf{P}]$ and $\mathcal{E}[\mathbf{Q}]$.

Therefore, the critical plastic modulus for coalescence of eigenvalues is

$$\boxed{g^C_{cr} = \max_{i=1,2,3} \frac{(\mathcal{E}[\mathbf{P}])_i(\mathcal{E}[\mathbf{Q}])_i}{\lambda+\mu},} \tag{194}$$

where $\mathcal{E}$ has the isotropic form and the index i, not summed, denotes principal components of $\mathcal{E}[\mathbf{P}]$ and $\mathcal{E}[\mathbf{Q}]$ (in the same reference system).

To summarize with the above specific example at hand, for deviatoric associativity, complex eigenvalues of the acoustic tensor are excluded, but coalescence of three eigenvalues may be verified. When this coalescence occurs and with reference to the above example, Bigoni and Loret (1999) have shown that a perturbation in terms of a small (appropriate) elastic anisotropy superimposed on the isotropic elastic law is sufficient to trigger flutter. Therefore, even if for the considered model complex eigenvalues are excluded, flutter as induced by physically motivated perturbations is possible and the critical condition corresponds to coalescence of the three eigenvalues of the acoustic tensor.

When coalescence is considered, Bigoni and Loret (1999) have shown that this situation may occur even if the constitutive operator is positive definite, a situation similar to what happen with the Ziegler double pendulum, where flutter occurs in the absence of any static bifurcation.

4 Concluding remarks on flutter instability in structures and solids

Flutter instability has been shown to be related to friction in both structures (where a follower force may be induced by higly anisotropic Coulomb friction) and elastoplastic solids (where frictional terms introduce a lack of symmetry in the constitutive equations).

For structural systems, numerical simulations which keep into account all nonlinearities (included those related to frictional contact) show that flutter initially corresponds to an oscillation blowing-up in time (as the linearized solution correctly predicts), but later this oscillation reaches a limit cycle, so that the structure behaves as a self-oscillating device. This behaviour is fully confirmed by experiments and can be considered indisputable.

For solids the situation is more complex. Available analytical solutions based on linearization predict the possibility of flutter as induced by nonassociativity of the plastic flow. In this context, flutter is understood in terms of waves blowing-up during propagation. Numerical evidences of flutter are still inconclusive both in showing a clear blowing-up and in predicting the achievement of a limit cycle.

The blowing-up of a signal during its propagation in a solid should not be too surprising, as materials obeying elastoplasticity with nonassociative flow rule have been shown to produce useful energy in closed loading cycles (Petryk, 1985). This circumstance does not necessarily violate conservation of energy, because a release of energy can be produced at the expense of the strain energy stored in the material in connection with the presence of initial prestress (always needed to generate plastic flow).

Analysis of constitutive models describing the behaviour of granular materials (Gajo et al., 2004) reveals that flutter instability should be considered more common than one could expect, a fact in agreement with the observation that granular matter is prone to unstable releases of energy. However, due to the effects of nonlinearities, the instability of flutter could be less 'explosive' than the exponential blow-up predicted by the linearized analysis.

Although experimental results indisputably showing flutter in a continuum are not available, there is evidence of oscillatory instabilities occurring in different situations involving the mechanics of granular materials and pointing to flutter instability.

One of these instabilities is responsible of the so-called 'singing (or squeaking) sand', a phenomenon known since a long time (it was reported by Marco Polo in his *Il milione* and by Charles Darwin in his *Voyage of the Beagle*) and consisting in the emission of an audible sound when certain types of sand are subject to shearing deformation. The grains of singing sands are coated with a silica layer and are of quartz or calcareous nature; the grain-size distribution is often uniform, and the grains roughly rounded. All these elements suggest that the squeaking of the sand is strictly related to intergranular friction, which is indeed the key element accounted for in the current models of this phenomenon (Andreotti and Bonneau, 2009; Dagois-Bohy et al., 2012). Sound emissions have also be noticed during straining of other granular materials such as snow (Patitsas, 2015). In all cases the frictional nature of the material and the vibrational origin of the phenomenon suggest a connection to flutter instability in a continuum.

Another phenomenon which can be thought to be in relation with flutter instability in solids is the so-called 'silo music' and 'silo quake', occurring during discharge of granular matter stored in silos. These structures fail with a much higher frequency than other industrial equipments (Carson and Holmes, 2003), frequently develop localized buckling (Fig. 24) and may also collapse, leading to loss of use.

During the operational life of silos, vibrations and repeated quakes occur

In CISM Lecture Notes No. 586 "Dynamic Stability and Bifurcation in Nonconservative Mechanics" (Ch. 1), edited by:
D. Bigoni and O. Kirillov, Springer, ISBN 978-3-319-93721-2, doi 10.1007/978-3-319-93722-9

Figure 24. Local buckling in two silos (near Bazzano, Italy).

at characteristic frequencies, leading to noise and even strong acoustic emission (nicknamed 'music'). These vibrations have relations with the failure of the structure and therefore have been thoroughly analyzed (Muite et al., 2004; Tejchman and Gudehus, 1993; Wilde et al., 2010). Several mechanical effects have been evidenced: (i.) resonant interactions between granular matter and silo structure, (ii.) formation of arch mechanisms in the granular body and (iii.) stick-slip motion at the interface between container and contained. Flutter instability may certainly play a role in this phenomenology.

Acknowledgments. Financial support from the ERC advanced grant

ERC-2013-ADG-340561-INSTABILITIES is gratefully acknowledged.

Bibliography

G.G. Adams. Self-excited oscillations of two elastic half-spaces sliding with a constant coefficient of friction. *J. Appl. Mech.*, 62:867–872, 1995.

B. Andreotti and L. Bonneau. Booming dune instability. *Phys. Rev. Letters*, 103:238001, 2009.

B. Audoly and Y. Pomeau. *Elasticity and Geometry.* Oxford University Press, 2010. ISBN 978-0-1985-0625-6.

M. Beck. Die knicklast des einseitig eingespannten, tangential gedrückten stabes. *Z. Angew. Math. Phys.*, 3:225–228, 1952.

D. Bigoni. On flutter instability in elastoplastic constitutive models. *Int. J. Solids Structures*, 32:3167–3189, 1995.

D. Bigoni. *Nonlinear Solid Mechanics Bifurcation Theory and Material Instability.* Cambridge University Press, 2012.

D. Bigoni and B. Loret. Effects of elastic anisotropy on strain localization and flutter instability in plastic solids. *J. Mech. Phys. Solids* , 47:1409–1436, 1999.

D. Bigoni and G. Noselli. Experimental evidence of flutter and divergence instabilities induced by dry friction. *J. Mech. Phys. Solids* , 59:2208–2226, 2011.

D. Bigoni and H. Petryk. A note on divergence and flutter instabilities in elastic-plastic materials. *Int. J. Solids Structures*, 39:911–926, 2002.

D. Bigoni and J.R. Willis. *A dynamical interpretation of flutter instability.* A.A. Balkema, Rotterdam, 1994.

D. Bigoni and D. Zaccaria. On eigenvalues of the acoustic tensor in elastoplasticity. *Eur. J. Mechanics-A/Solids* , 13:621–638, 1994.

D. Bigoni, B. Loret, and E. Radi. Localization of deformation in plane elastic-plastic solids with anisotropic elasticity. *J. Mech. Phys. Solids* , 48:1441–1466, 2000.

D. Bigoni, D. Misseroni, G. Noselli, and D. Zaccaria. *Surprising instabilities of simple elastic structures*, pages 1–14. Wiley, 2014.

D. Bigoni, F. Bosi, D. Misseroni, F. Dal Corso, and G. Noselli. *New phenomena in nonlinear elastic structures: from tensile buckling to configurational forces.* Springer, 2015. ISBN 978-3-7091-1876-4.

D. Bigoni, D. Misseroni, M. Tommasini, O. Kirillov, and G. Noselli. Detecting singular weak-dissipation limit for flutter onset in reversible systems. *Phys. Rev. E*, 97:023003, 2018.

V.V. Bolotin. *Nonconservative problems of the theory of elastic stability.* Pergamon Press, New York, 1963.

O. Bottema. The routh-hurwitz condition for the biquadratic equation. *Indagationes Mathematicae*, 18:403–406, 1956.

R.M. Brannon. *Elements of phenomenological plasticity: Geometrical insight, computational algorithms, and topics in shock physics*, pages 225–274. Springer Berlin Heidelberg, 2007.

R.M. Brannon and W.J. Drugan. Influence of non-classical elastic-plastic constitutive features on shock wave existence and spectral solutions. *J. Mech. Phys. Solids* , 41:297–330, 1993.

A. Broman. *Introduction to partial differential equations.* Dover, 1970.

J. Burghardt and R.M. Brannon. Nonuniqueness and instability of classical formulations of nonassociated plasticity, ii: Effect of nontraditional plasticity features on the sandler-rubin instability. *J. Mech. Materials Structures*, 10:149–166, 2015.

J.W. Carson and T. Holmes. Silo failures: why do they happen? *Task Quarterly*, 4:499–512, 2003.

S. Dagois-Bohy, S. Courrech du Pont, and S. Douady. Singing-sand avalanches without dunes. *Geoph. Res. Letters* , 39(20), 2012.

J.P. Den Hartog. Forced vibrations with combined coulomb and viscous friction. *ASME APM-53*, pages 107–115, 1931.

J.P. Den Hartog. *Mechanical vibrations.* McGraw-Hill, 1956.

O. Doaré and S. Michelin. Piezoelectric coupling in energy-harvesting fluttering flexible plates: linear stability analysis and conversion efficiency. *J. Fluids Structures*, 27:1357–1375, 2011.

F. D'Annibale, G. Rosi, and A. Luongo. Controlling the limit-cycle of the ziegler column via a tuned piezoelectric damper. *Mathematical Problems in Engineering*, 2015.

I. Elishakoff. Controversy associated with the so-called "follower force": critical overview. *Appl. Mech. Rev.*, 58:117–142, 2005.

A. Gajo, D. Bigoni, and D. Muir Wood. Multiple shear band development and related instabilities in granular materials. *J. Mech. Phys. Solids* , 52:2683–2724, 2004.

K.F. Graff. *Wave Motion in Elastic Solids.* Ohio State University Press, 1975.

G. Herrmann. Dynamics and stability of mechanical systems with follower forces. tech. rept. nasa cr-1782, 1971.

G. Herrmann, S. Nemat-Nasser, and S.N. Prasad. Models demonstrating instability of nonconservative dynamical systems. tech. rept. no. 66-4, 1966.

R. Hill. Acceleration waves in solids. *J. Mech. Phys. Solids* , 10:1–16, 1962.

R.A. Ibrahim. Friction-induced vibration, chatter, squeal, and chaos part i: Mechanics of contact and friction. *Appl. Mech. Rev*, 47:209–226, 1994a.

R.A. Ibrahim. Friction-induced vibration, chatter, squeal, and chaos part ii: Dynamics and modeling. *Appl. Mech. Rev*, 47:227–253, 1994b.

A. Jenkins. Self-oscillation. *Physics Reports*, 525:167–222, 2013.

O.N. Kirillov. A theory of the destabilization paradox in non-conservative systems. *Acta Mech.*, 174:145–166, 2005.

O.N. Kirillov. *Nonconservative Stability Problems of Modern Physics*. De Gruyter, 2013.

O.N. Kirillov and F. Verhulst. Paradoxes of dissipation-induced destabilization or who opened whitney's umbrella? *Z. Angew. Math. Mech.*, 90: 462–488, 2010.

W.T. Koiter. Unrealistic follower forces. *J. Sound and Vibration* , 194: 636–638, 1996.

R. Krechetnikov and J.E. Marsden. Dissipation-induced instabilities in finite dimensions. *Reviews Modern Phys*, 79:519–553, 2007.

M. Kröger, M. Neubauer, and K. Popp. Experimental investigation on the avoidance of self-excited vibrations. *Phil. Trans. R. Soc.A*, 366:785–810, 2008.

B. Loret. Does deviation from deviatoric associativity lead to the onset of flutter instability? *J. Mech. Phys. Solids* , 40:1363–1375, 1992.

B. Loret, J.H. Prevost, and O. Harireche. Loss of hyperbolicity in elastic-plastic solids with deviatoric associativity. *Eur. J. Mechanics-A/Solids* , 9:225–231, 1990.

B. Loret, F.M.F. Simões, and J.A.C. Martins. *Flutter instability and ill-posedness in solids and fluid-saturated porous media*, pages 109–207. Springer-Verlag, Wien-New York, 2000.

I. Lottati and I. Elishakoff. A new 'destabilization' phenomenon: influence of rotary damping. *Ingenieur-Archiv*, 57:413–419, 1987.

A.E.H. Love. *A treatise on the mathematical theory of elasticity*. Cambridge University Press, 1927.

G. Maier. A minimum principle for incremental elastoplasticity with nonassociated flow-laws. *J. Mech. Phys. Solids* , 18:319–330, 1970.

J. Mandel. Ondes plastiques dans un milieu indéfini à trois dimensions. *J. de Mécanique*, 1:3–30, 1962.

J. Mandel. *Conditions de stabilité et postulat de Drucker*, pages 58–68. Springer, Berlin, 1966.

J.A.C. Martins, S. Barbarin, M. Raous, and A. Pinto da Costa. Dynamic stability of finite dimensional linearly elastic systems with unilateral contact and coulomb friction. *Comput. Meth. Appl. Mech. Engrg.*, 177:289–328, 1999.

Z. Mróz. Non-associated flow laws in plasticity. *J. de Mechanique*, 2:21–42, 1963.

Z. Mróz. On forms of constitutive laws for elastic-plastic solids. *Arch. Mech. Stosowanej*, 18:1–34, 1966.

B.K. Muite, S.F. Quinn, S. Sundaresan, and K.K. Rao. Silo music and silo quake: granular flow-induced vibration. *Powder Tech.*, 145:190–202, 2004.

M. Neubauer, C.C. Neuber, and K. Popp. Control of stick-slip vibrations. In *Proc. of IUTAM Symposium on Vibration Control of Nonlinear Mechanisms and Structures, Munich, Germany*, volume 145, pages 223–232, 2005.

Q.S. Nguyen. *Stabilité des structures élastiques*. Springer-Verlag, 1995.

Q.S. Nguyen. Instability and friction. *Comptes Rendus Mécanique*, 331: 99–112, 2003.

M.P. Paidoussis. *Fluid-Structure Interactions*, volume 1 and 2. Elsevier, 2nd edition, 2014.

A.J. Patitsas. Snow sounds when rubbing or impacting a snow bed. *Can. J. Phys.*, 93:1302–1309, 2015.

H. Petryk. On stability and symmetry conditions in time-independent plasticity. *Arch. Mech.*, 37:503–520, 1985.

A. Pflüger. *Stabilitätsprobleme der Elastostatik*. Springer, Berlin, 1950.

A. Pflüger. Zur stabilität des tangential gedruckten stabes. *Z. Angew. Math. Mech.*, 5(191), 1955.

A. Piccolroaz, D. Bigoni, and J.R. Willis. A dynamical interpretation of flutter instability in a continuous medium. *J. Mech. Phys. Solids* , 54: 2391–2417, 2006.

W. Prager. Recent developments in the mathematical theory of plasticity. *J. Appl. Phys.*, 20:235–241, 1949.

T. Pucik, R.M. Brannon, and J. Burghardt. Nonuniqueness and instability of classical formulations of nonassociated plasticity, i: Case study. *J. Mech. Materials Structures*, 10:123–148, 2015.

E. Radi, D. Bigoni, and A. Tralli. On uniqueness for frictional contact rate problems. *J. Mech. Phys. Solids* , 47:275–296, 1999.

B. Raniecki. *Ordinary waves in inviscid plastic media*. Springer-Verlag, Wien, 1976.

E.L. Reiss. *Column buckling: An elementary example of bifurcation*, pages 1–16. W.A. Benjamin Inc., New York, 1969.

J.R. Rice. *The localization of plastic deformation*, pages 207–220. North-Holland, Amsterdam, 1977.

J.R. Rice and A.L. Ruina. Stability of steady frictional slipping. *J. Appl. Mech.*, 50:343–349, 1983.

I. Sandler and D. Rubin. *The consequences of non-associated plasticity in dynamic problems*, pages 345–353. Elsevier Science Publishing Co. Inc., Amsterdam, 1987.

F.M.F. Simões and J.A.C. Martins. Instability and ill-posedness in some friction problems. *Int. J. Eng. Sci.*, 36:1265–1293, 1998.

Y. Sugiyama, K. Katayama, and S. Kinoi. Flutter of a cantilevered column under rocket thrust. *J. Aerospace Eng.*, 8:9–15, 1995.

Y. Sugiyama, K. Katayama, K. Kiriyama, and B.J. Ryu. Experimental verification of dynamic stability of vertical cantilevered columns subjected to a sub-tangential force. *J. Sound and Vibration* , 236:193–207, 2000.

J. Tejchman and G. Gudehus. Silo music and silo-quake experiments and a numerical cosserat approach. *Powder Tech.*, 76:201–212, 1993.

K. Wilde, J. Tejchman, M. Rucka, and M. Niedostatkiewicz. Experimental and theoretical investigations of silo music. *Powder Tech.*, 198:38–48, 2010.

H. Ziegler. Die stabilitätskriterien der elastomechanik. *Ingenieur-Archiv*, XX:49–56, 1952.

H. Ziegler. Linear elastic stability. a critical analysis of methods. *Z. Angew. Math. Phys.*, 4:89–121, 1953.

H. Ziegler. On the concept of elastic stability. *Advances in Applied Mechanics* , 4:351–403, 1956.

H. Ziegler. *Principles of structural stability.* Birkhäuser Verlag, Basel und Stuttgart, 1977.